

BPS Wilson Loops on S^2 at Higher Loops

Donovan Young

*Humboldt-Universität zu Berlin, Institut für Physik,
Newtonstraße 15, D-12489 Berlin, Germany*

`dyoung@physik.hu-berlin.de`

Abstract

We consider supersymmetric Wilson loops of the variety constructed by Drukker, Giombi, Ricci, and Trancanelli, whose spatial contours lie on a two-sphere. Working to second order in the 't Hooft coupling in planar $\mathcal{N} = 4$ Supersymmetric Yang-Mills Theory (SYM), we compute the vacuum expectation value of a wavy-latitude and of a loop composed of two longitudes. We evaluate the resulting integrals numerically and find that the results are consistent with the zero-instanton sector calculation of Wilson loops in 2-d Yang-Mills on S^2 performed by Bassetto and Griguolo. We also consider the connected correlator of two distinct latitudes to third order in the 't Hooft coupling in planar $\mathcal{N} = 4$ SYM. We compare the result in the limit where the latitudes become coincident to a perturbative calculation in 2-d Yang-Mills on S^2 using a light-cone Wu-Mandelstam-Leibbrandt prescription. We are not able to calculate the SYM result at the required order in the separation between the latitudes necessary for a match with 2-d Yang-Mills; the result, however, does not preclude such a match.

1 Introduction and results

The study of Wilson loops in $\mathcal{N} = 4$ supersymmetric Yang-Mills theory [1, 2] has provided a unique and rich avenue for probing the AdS/CFT correspondence [3] as well as the theory itself. Certain loops which respect some of the supersymmetries of the underlying theory have been analyzed with great success. Loops with arbitrary shape may be constructed with enough supersymmetry to yield trivial vacuum expectation values [6, 7], a result which is also well understood in string theory [8]. Supersymmetric Wilson loops with non-trivial vacuum expectation values are also of prime interest. The 1/2 BPS circle was understood early-on to be described by a zero-dimensional theory - the celebrated Hermitian matrix model of Erickson, Semenoff, and Zarembo [9]. This matrix model appears to encode the object entirely [10], including the string-side manifestation of large representations [11–18] and two-point functions with local operators [19–22]. Indeed, a recent paper [23] has claimed a proof of this result. Recently, a much larger class of supersymmetric loops with non-trivial expectation values were discovered [24]. These loops lie on an S^3 and are generically 1/16 BPS. An important subclass of those loops lie on a great S^2 inside the S^3 . It has been suggested by their discoverers that these Wilson loops might be captured exactly by a reduced two-dimensional model which one could describe roughly as a perturbative pure Yang-Mills theory on S^2 , where the Wu-Mandelstam-Leibbrandt [25–27] prescription for the regularization of the propagator is used [28, 29]. We will refer to this simply as the “reduced 2-d model”.

The Wilson loop on S^2 proposed by [24] is given by

$$W = \frac{1}{N} \text{Tr} \mathcal{P} \exp \oint d\tau \left(i \dot{x}^i A_i + \epsilon_{ijk} x^j \dot{x}^k M_I^i \Phi_I \right) \quad (1)$$

where $x^i(\tau)$ (where $i = 1, \dots, 3, I = 1, \dots, 6$) is a closed path on S^2 , and M_I^i is a 3×6 matrix satisfying $MM^T = 1$ and which we will take to be $M_i^i = 1$ (no summation implied) and all other entries zero. The existing evidence that this object might be captured by a reduced 2-d model has been presented in [28] and [29]. Here we will give a short review of those results. One of the most compelling observations is that the combined scalar and gauge field (Feynman gauge) propagator joining two points x and y on the loop (the so-called “loop-to-loop propagator”) is given by

$$D_{4d} \propto \frac{g^2}{R^2} \left(\frac{1}{2} \delta_{ij} - \frac{(x-y)_i (x-y)_j}{(x-y)^2} \right), \quad i, j = 1, 2, 3 \quad (2)$$

where R is the radius of the S^2 . This indeed is the propagator of pure 2-d Yang-Mills in a certain gauge, with coupling $g_{2d}^2 = -g^2/(4\pi R^2)$. Using this one can prove via Stokes theorem that for a general closed contour on S^2

$$\langle W \rangle = 1 + \lambda \frac{\mathcal{A}_1 \mathcal{A}_2}{2\mathcal{A}^2} + \mathcal{O}(\lambda^2), \quad (3)$$

where $\lambda = g^2 N$, and \mathcal{A}_1 and \mathcal{A}_2 are the two areas of the S^2 bounded by the Wilson loop, while \mathcal{A} is their sum, the total sphere area. This result can then be compared to that for a Wilson loop of arbitrary path in 2-d Yang-Mills on S^2 in the zero-instanton

sector, as calculated by Bassetto and Griguolo [32] using the expansion of Witten [33, 34]¹. Under the proposed relation between the 2-d and 4-d coupling, that result reads²

$$\langle W \rangle = \frac{1}{N} L_{N-1}^1 \left(-g^2 \frac{\mathcal{A}_1 \mathcal{A}_2}{\mathcal{A}^2} \right) \exp \left(\frac{g^2}{2} \frac{\mathcal{A}_1 \mathcal{A}_2}{\mathcal{A}^2} \right), \quad (4)$$

and agrees with (3) to first order in λ . In fact the 1/2 BPS circular Wilson loop of $\mathcal{N} = 4$ supersymmetric Yang-Mills theory, and further, Drukker's 1/4 BPS generalization of it [30] are special cases of (1). As mentioned above, there exists a wealth of evidence (both at weak and at strong coupling, and especially for the 1/2 BPS circle) that these loops are described exactly by a Hermitian matrix model, whose result for $\langle W \rangle$ agrees precisely with (4). Finally, the authors in [29] present a strong coupling calculation of $\langle W \rangle$ for a Wilson loop composed of two longitudes separated by an arbitrary angle using the AdS/CFT correspondence. That result is also in agreement with (4).

In the decompactification limit $R \rightarrow \infty$, (4) agrees with the perturbative calculation of Staudacher and Krauth [31], performed by summing-up ladder diagrams in the light-cone Wu-Mandelstam-Leibbrandt prescription for 2-d Yang-Mills in the plane. The “2-d reduced model” proposed in [29] is essentially the same idea; albeit on S^2 rather than the plane and in a different gauge. They first give an action on an S^2 parametrized by complex coordinates z, \bar{z}

$$x^i = \frac{1}{1 + z\bar{z}} (z + \bar{z}, -i(z - \bar{z}), 1 - z\bar{z}). \quad (5)$$

Beginning with generalized Feynman gauge with gauge parameter $\xi = -1$ they propose the following Lagrangian density

$$\mathcal{L} = \frac{\sqrt{g}}{g_{2d}^2} \left[\frac{1}{4} (F_{ij}^a)^2 - \frac{1}{2} (\nabla^i A_i^a)^2 \right] \quad (6)$$

where g is the determinant of the S^2 metric (i.e. $ds^2 = 4dzd\bar{z}/(1 + z\bar{z})^2$). This leads to propagators for the A_z and $A_{\bar{z}}$ fields as follows

$$\begin{aligned} \langle A_z(z) A_z(w) \rangle &= \frac{g_{2d}^2}{\pi} \frac{1}{(1 + z\bar{z})} \frac{1}{(1 + w\bar{w})} \frac{\bar{z} - \bar{w}}{z - w} \\ \langle A_{\bar{z}}(z) A_{\bar{z}}(w) \rangle &= \frac{g_{2d}^2}{\pi} \frac{1}{(1 + z\bar{z})} \frac{1}{(1 + w\bar{w})} \frac{z - w}{\bar{z} - \bar{w}} \end{aligned} \quad (7)$$

which agree with (2) when written in the original cartesian coordinates. In the decompactification limit these propagators coincide with the Wu-Mandelstam-Leibbrandt, light-cone propagators used by Staudacher and Krauth, up to a factor of 2. However one can change here to a light-cone gauge, setting $A_{\bar{z}} = 0$; this gauge choice just

¹In the work [36], it was shown that in summing this expansion, instantons are crucial for the recovery of strong coupling physics [35].

² L_n^m is the Laguerre polynomial $L_n^m(x) = 1/n! \exp[x] x^{-m} (d/dx)^n (\exp[-x] x^{n+m})$.

results in twice the first propagator in (7). This light-cone gauge propagator takes on the form

$$D_{4d} + iD_0 \tag{8}$$

where D_{4d} is the loop-to-loop propagator from $\mathcal{N} = 4$ SYM in Feynman gauge (i.e. (2)) while iD_0 is a new imaginary piece generated by the gauge transformation. Employing this gauge affords a great simplification in Feynman diagrams since interactions are clearly removed; one needs only consider the sum of ladder diagrams. These might reproduce (4) for single Wilson loops on S^2 . For the connected correlator of two Wilson loops, one can simply compare $\mathcal{N} = 4$ SYM results to ladder diagrams.

It is the purpose of this paper to explore the connection of the Wilson loops (1) to the proposed reduced 2-d model further. We consider the vacuum expectation value (VEV) of the Wilson loop constructed in [29] consisting of two longitudes to second order in the 't Hooft coupling. The resulting integrals involve Feynman parameters as well as integrations over the longitudes themselves. We find that for angles away from zero separating the longitudes, numerical integration produces accurate results. These are in excellent agreement with (4). We continue to the same calculation for a “wavy-latitude”: a latitude with a sinusoidal wave of low period in the polar angle describing it, see figure 1. Using the same techniques, we similarly find excellent agreement with (4), and for a continuous range of wave amplitudes. We also consider the connected

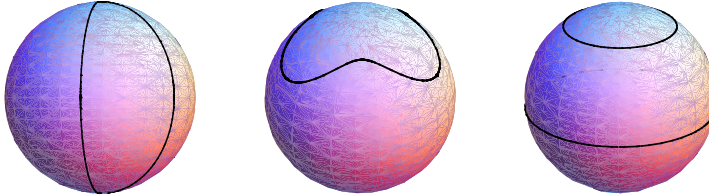


Figure 1: The three geometries of Wilson loops on S^2 we consider: two longitudes, wavy-latitude, and two latitudes.

correlator of two distinct latitudes to third order in the 't Hooft coupling. In this case we cannot compare to the Bassetto and Griguolo result, as that result is valid for the VEV of a single Wilson loop and not a connected correlator of two. Instead we compare to the reduced 2-d model of [29] presented above, in light-cone gauge. The reduced model produces results which are consistent with the result from planar $\mathcal{N} = 4$ SYM at leading order (second order) in the 't Hooft coupling. At the next order, i.e. third order in the 't Hooft coupling, we attempt to make a comparison in the limit where the latitudes becomes coincident. We find that we are unable to calculate the result at the necessary order in the separation of the latitudes to test for a match with the reduced model, but the result also does not preclude the existence of such a match.

The structure of the paper is as follows. In section 2 we calculate the VEV of single Wilson loops; we consider the case of two longitudes and of a wavy latitude. In section 3 we compare the connected correlator of two latitudes, as calculated in

$\mathcal{N} = 4$ SYM to the expectation from the 2-d reduced model in light-cone gauge. We conclude with a discussion of the results in section 4. The details of the calculations, which are very complicated, have been included in the appendices. As this manuscript was being readied for publication [37] appeared which has some overlap with section 2.1.

Notes concerning v4

In the earlier versions of this manuscript an error was present in the analysis of the coincident limit of the correlator calculation. The original claim was that there was a mismatch between the two-dimensional Yang-Mills result and the one coming from $\mathcal{N} = 4$ SYM in the case of the correlator. We have discovered that the error lay in taking the coincident limit - having fixed the error we find that we cannot get results at the same order in the separation between the latitudes which were advertised in previous versions.

2 Calculations of $\langle W \rangle$ at $\mathcal{O}(\lambda^2)$

We consider the VEV of a Wilson loop of the variety (1). As explained in the introduction, at $\mathcal{O}(\lambda)$ these loops have been proven to be captured by (4). We would like to understand whether this agreement persists at the next order in perturbation theory. A two-loop calculation was performed for the 1/2 BPS circle in [9]; we follow that calculation closely and refer the reader there for conventions and notation. We use the Euclidean action of $\mathcal{N} = 4$ SYM in Feynman gauge and dimensional regularization.

There are three types of diagrams contributing to $\langle W \rangle$ at $\mathcal{O}(\lambda^2)$. The simplest are the rainbow/ladder graphs - those graphs without interaction vertices. The next contributions come from diagrams with interaction vertices, these are shown schematically in figure 2. In what follows we will assume smooth Wilson loop contours; the

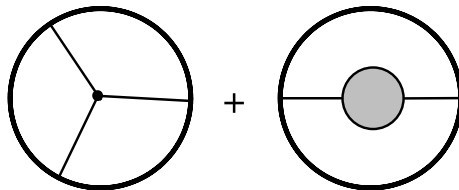


Figure 2: The two-loop, non-ladder/rainbow diagrams contributing to $\langle W \rangle$. The Wilson loop is indicated by the outer circle. Internal solid lines refer to scalar and gauge fields, while the greyed-in bubble represents the one-loop correction to the propagator.

case of the two longitudes will be slightly different. We may generalize eq. (13) of [9], which gives the contribution from the diagram on the left in figure 2. In keeping with their notation, we call this quantity Σ_3

$$\Sigma_3 = -\frac{\lambda^2}{4} \oint d\tau_1 d\tau_2 d\tau_3 \epsilon(\tau_1 \tau_2 \tau_3) D(\tau_1, \tau_3) \dot{x}_2 \cdot \partial_{x_1} G(x_1, x_2, x_3) \quad (9)$$

where³ we have used $D(\tau_1, \tau_3)$ to refer to the numerator of the loop-to-loop propagator, i.e. in our case $D(\tau_1, \tau_2) = (\dot{x}_1 \cdot \dot{x}_2)(x_1 \cdot x_2 - 1) - (x_1 \cdot \dot{x}_2)(x_2 \cdot \dot{x}_1)$, while the function G is as defined in [9]

$$G(x_1, x_2, x_3) = \frac{\Gamma(2\omega - 3)}{2^6 \pi^{2\omega}} \int_0^1 d\alpha d\beta d\gamma (\alpha\beta\gamma)^{\omega-2} \delta(1 - \alpha - \beta - \gamma) \times \frac{1}{[\alpha\beta(x_1 - x_2)^2 + \beta\gamma(x_2 - x_3)^2 + \alpha\gamma(x_1 - x_3)^2]^{2\omega-3}} \quad (10)$$

where the number of dimensions is given by $d = 2\omega$, so that the physical dimension is at $\omega = 2$. Using the fact that⁴

$$\oint d\tau_1 d\tau_2 d\tau_3 \frac{d}{d\tau_1} \left(\epsilon(\tau_1 \tau_2 \tau_3) D(\tau_1, \tau_3) G(x_1, x_2, x_3) \right) = 0 \quad (11)$$

one may prove that

$$\frac{\lambda^2}{2} \oint d\tau_1 d\tau_3 \frac{D(\tau_2, \tau_3)}{G|_{\tau_1=\tau_2}} = -\frac{\lambda^2}{4} \oint d\tau_1 d\tau_2 d\tau_3 \epsilon(\tau_1 \tau_2 \tau_3) \partial_{\tau_1} \left(D(\tau_1, \tau_3) G \right). \quad (12)$$

In fact, as shown in [9], on the physical dimension, the LHS of the expression (12) (which is divergent) reduces to exactly minus the contribution of the diagram pictured on the right of figure 2. The sum of the two diagrams is therefore given by (calling the contribution of the second diagram Σ_2)

$$\Sigma_3 + \Sigma_2 = -\frac{\lambda^2}{4} \oint d\tau_1 d\tau_2 d\tau_3 \epsilon(\tau_1 \tau_2 \tau_3) \left[D(\tau_1, \tau_3) \dot{x}_2 \cdot \partial_{x_1} G - \partial_{\tau_1} \left(D(\tau_1, \tau_3) G \right) \right] \quad (13)$$

which for the 1/2 BPS circle [9], and for the latitude [30] is easily proven to be zero. As long as the Wilson loop under consideration is finite at one-loop, i.e.

$$\oint d\tau_1 d\tau_2 \frac{D(\tau_1, \tau_2)}{(x_1 - x_2)^2} = \text{finite} \quad (14)$$

it also easy to see that (13) is finite. We will discuss this point further in section 2.3.

Our strategy is to evaluate the rainbow/ladders and the quantity (13) using numerical integration, and to compare to the expectation from (4). Expanding that expression in the large- N , small- λ limit, one finds

³The symbol $\epsilon(\tau_1 \tau_2 \tau_3)$ refers to antisymmetric path-ordering. It is given by +1 for $\tau_1 > \tau_2 > \tau_3$ and is totally antisymmetric in the τ_i .

⁴This is the relation which must be modified for curves which are piecewise defined.

$$\langle W \rangle = 1 + \frac{\hat{\lambda}}{8} \mathcal{A}_1(4\pi - \mathcal{A}_1) + \frac{\hat{\lambda}^2}{192} (\mathcal{A}_1(4\pi - \mathcal{A}_1))^2 + \dots \quad (15)$$

where we have defined $\hat{\lambda} \equiv \lambda/(4\pi^2)$ and where \mathcal{A}_1 is either of the areas enclosed by the Wilson loop on S^2 .

2.1 Two longitudes

We consider the Wilson loop defined by (1) consisting of two longitudes separated by an azimuthal angle δ on S^2 , as pictured in figure 3. This loop was first constructed

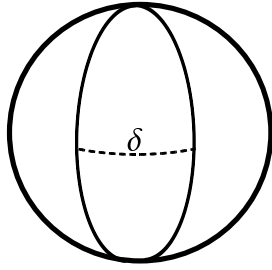


Figure 3: A Wilson loop composed of two longitudes.

in [29] and it is relatively straightforward to prove that it is indeed captured by (4) to first order in the 't Hooft coupling directly. The longitudes are given by

$$\begin{aligned} x^i &= (\sin t, 0, \cos t), \quad 0 \leq t < \pi \\ x^i &= (-\cos \delta \sin t, -\sin \delta \sin t, \cos t), \quad \pi \leq t < 2\pi \end{aligned} \quad (16)$$

where the first longitude couples to the scalar field Φ_2 , and the second to $-\Phi_2 \cos \delta + \Phi_1 \sin \delta$. The combined gauge field and scalar propagator joining two points on the same longitude is a constant $\lambda/(4\pi^2) \times 1/2 = \hat{\lambda}/2$, while that joining the two longitudes is given by

$$P(t_1, t_2) = \hat{\lambda} \frac{-\dot{x}_1 \cdot \dot{x}_2 - \cos \delta}{2(1 - x_1 \cdot x_2)} = \hat{\lambda} \frac{\cos \delta \cos t_1 \cos t_2 - \sin t_1 \sin t_2 - \cos \delta}{2(1 + \cos \delta \sin t_1 \sin t_2 - \cos t_1 \cos t_2)}. \quad (17)$$

We begin with those rainbow/ladder graphs which do not involve the propagator $P(t_1, t_2)$; these are pictured in figure 4. We find that these diagrams yield the following

$$\begin{aligned} \frac{\hat{\lambda}^2}{4} &\left[2 \int_0^\pi dt_1 \int_0^{t_1} dt_2 \int_0^{t_2} dt_3 \int_0^{t_3} dt_4 \left(\frac{1}{2}\right)^2 + 2 \int_\pi^{2\pi} dt_1 \int_\pi^{t_1} dt_2 \int_\pi^{t_2} dt_3 \int_\pi^{t_3} dt_4 \left(\frac{1}{2}\right)^2 \right. \\ &\left. + \int_\pi^{2\pi} dt_1 \int_\pi^{t_1} dt_2 \int_0^\pi dt_3 \int_\pi^{t_3} dt_4 \left(\frac{1}{2}\right)^2 \right] = \frac{\hat{\lambda}^2}{16} \left[(2+2) \cdot \frac{\pi^4}{4!} + \left(\frac{\pi^2}{2!}\right)^2 \right] = \frac{5\hat{\lambda}^2}{192} \pi^4 \end{aligned} \quad (18)$$

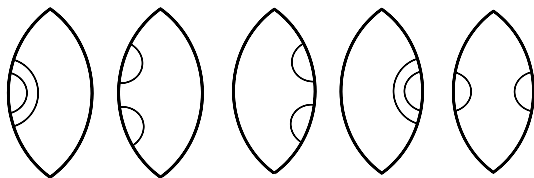


Figure 4: A subset of the two-loop diagrams.

where the leading factor of $1/4$ comes from the traces over gauge group matrices, while the $1/4!$ which comes from the expansion of the Wilson loop to fourth order has been eliminated by the $4!$ equivalent orderings of the fields in that expansion. The next class of two-loop rainbow/ladder diagrams contain the $P(t_1, t_2)$ propagator and are pictured in figure 5.

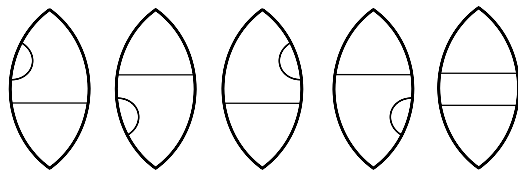


Figure 5: A (different) subset of the two-loop diagrams.

We find the result for these diagrams to be

$$\begin{aligned} \Lambda_2 \equiv & \frac{\hat{\lambda}^2}{2} \int_{\pi}^{2\pi} dt_1 \int_0^{\pi} dt_2 \int_0^{t_2} dt_3 \int_0^{t_3} dt_4 \left(\frac{1}{2} \right) \left(P(t_1, t_4) + P(t_1, t_2) \right) \\ & + \frac{\hat{\lambda}^2}{4} \int_{\pi}^{2\pi} dt_1 \int_{\pi}^{t_1} dt_2 \int_0^{\pi} dt_3 \int_0^{t_3} dt_4 P(t_1, t_4) P(t_2, t_3). \end{aligned} \quad (19)$$

There are two checks which we can make on the sum of two-loop rainbow/ladders. The first is at $\delta = 0$ where the longitudes lie atop one another with opposite orientation. Here the result should be zero, and is. The second is at $\delta = \pi$ where the longitudes degenerate to a great circle. Here the result should match that of the $1/2$ BPS circle, since there internal vertex diagrams cancel [9]. One can check that this test is also passed.

The expectation from (15) at two-loop order is easily seen to be $\hat{\lambda}^2 \delta^2 (2\pi - \delta)^2 / 12$. It is interesting to ask whether or not the sum of two-loop rainbow/ladder diagrams is already proportional to $\delta^2 (2\pi - \delta)^2$, even without the contribution of the internal vertex diagrams. Due especially to the last integral in (19), we need to resort to numerical integration in order to answer this question. As we will see the answer is no. The internal vertex diagrams, however, give a finite contribution which together with the rainbow/ladders, reproduces the prediction from (4). Due to the fact that this Wilson loop is piecewise defined, the interacting diagrams and their divergence

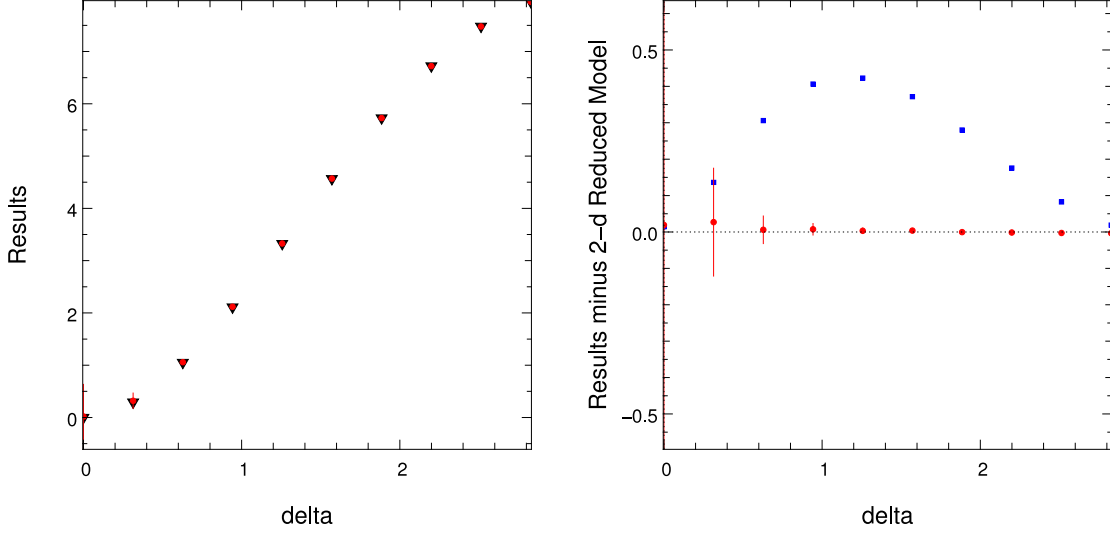


Figure 6: Two-loop results for a Wilson loop composed of two longitudes ($\hat{\lambda}$ is set to 1). In red dots the result of numerical integration is shown. In black triangles the expectation from (4) is plotted. On the right data including the result from only rainbow/ladder diagrams (blue squares) are plotted with the expectation from (4) subtracted.

cancellation is more subtle than that presented at the start of this section. We have relegated the details to appendix A. We find the following result for the finite remainder after the divergence cancellation

$$\Lambda_3 = -\frac{\hat{\lambda}^2}{16} \int_0^1 d\alpha d\beta d\gamma \delta(1 - \alpha - \beta - \gamma) \left[\int_\pi^{2\pi} d\tau_1 \int_0^\pi d\tau_2 \int_0^\pi d\tau_3 \epsilon(\tau_2 \tau_3) \frac{B_1 + B_2 + B_3}{\Delta^2} - \int_\pi^{2\pi} d\tau_1 \int_0^\pi d\tau_2 \frac{(1 + \sigma)(2 + c_1 + c_2)}{[\alpha\beta(1 + \sigma s_1 s_2 - c_1 c_2) + \beta\gamma(1 + c_2) + \alpha\gamma(1 + c_1)]} \right] \quad (20)$$

$$\begin{aligned} B_1 + B_2 + B_3 = & \alpha\gamma(\sigma^2 - 1) [2s_1(c_3 - c_2) - s_1 c_1(1 - \cos \tau_{23})] \\ & + \alpha\gamma(\sigma + 1)(s_2 - s_3)(c_3 - c_1) \\ & + \alpha\gamma(\sigma + 1) [\sin \tau_{13}^+ - \sin \tau_{12}^+ + \sin \tau_{23}] \\ & + \alpha\gamma(\sigma + 1) \sin \tau_{23}(1 - \cos \tau_{13}^+) + \beta\gamma(\sigma + 1)c_1 s_3(1 - \cos \tau_{23}) \end{aligned} \quad (21)$$

where we have introduced some shorthand $\sigma \equiv \cos \delta$, $c_i \equiv \cos \tau_i$, $s_i \equiv \sin \tau_i$, $\tau_{ij} \equiv \tau_i - \tau_j$, $\tau_{ij}^+ \equiv \tau_i + \tau_j$, and

$$\begin{aligned} \Delta = & \alpha\beta(1 + \sigma \sin \tau_1 \sin \tau_2 - \cos \tau_1 \cos \tau_2) + \beta\gamma(1 - \cos \tau_{23}) \\ & + \alpha\gamma(1 + \sigma \sin \tau_1 \sin \tau_3 - \cos \tau_1 \cos \tau_3). \end{aligned} \quad (22)$$

We have evaluated the complete result $5\hat{\lambda}^2\pi^4/192 + \Lambda_2 + \Lambda_3$ via numerical integration. The results are shown in figure 6 for a range of opening angles δ as red dots with estimated error bars. Also plotted as black triangles is the expectation from (4), i.e. $\hat{\lambda}^2 \delta^2(2\pi - \delta)^2/12$. On the right the results, including the rainbow/ladder contribution alone (i.e. $5\hat{\lambda}^2\pi^4/192 + \Lambda_2$) are plotted with the expectation from (4) subtracted. It is clear both that the rainbow/ladders fail to reproduce the expectation from (4), and that the addition of Λ_3 , at least for angles δ away from $\delta = 0$, reproduces them excellently. As $\delta = 0$ is approached the numerical integration is no longer reliable (as evidenced by the growing error bars). The reasons for this are discussed in section 2.3. We also note from (20) that Λ_3 vanishes exactly for $\delta = \pi$ when the longitudes degenerate to a circle; this is a consistency check against the known vanishing of interacting diagrams for the 1/2 BPS circle [9].

2.2 Wavy latitudes

We now consider (1) using a class of closed contours we refer to as “wavy latitudes”. They are given by

$$\vec{x}(\tau) = (\sin \theta(\tau) \cos \tau, \sin \theta(\tau) \sin \tau, \cos \theta(\tau)), \quad \theta(\tau) = \theta_0 + A \cos n\tau \quad (23)$$

where n is an integer. For $A = 0$ these loops reduce to the latitudes which were shown in [24] to be essentially the same (via a conformal transformation) as the 1/4 BPS circle of Drukker [30], and for which the 1/2 BPS circle is a special case. In figure 7, we have plotted the curves for $\theta_0 = \pi/4$, and A ranging from 0 to 0.3 for the cases $n = 2, 3$. The viewpoint is straight down the north pole of the sphere, i.e. the contours have been (flatly) projected into the x_1 - x_2 plane. The rainbow/ladder

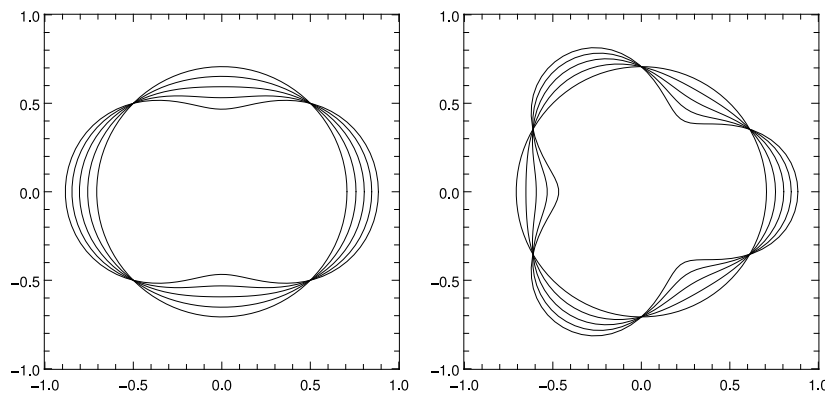


Figure 7: The contours (23) are plotted from the view-point straight down the north pole of the sphere (flat projection). Here $\theta_0 = \pi/4$ while A ranges from 0 to 0.3. On the left n has been set to 2, on the right $n = 3$.

contribution is given by

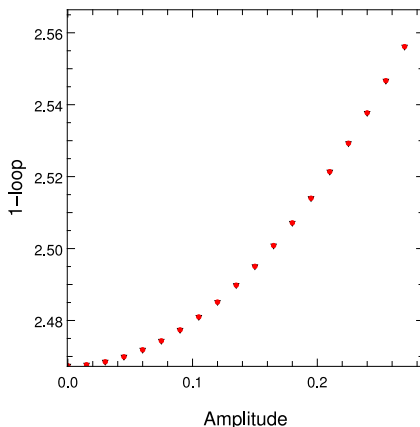


Figure 8: The coefficient of $\hat{\lambda}$ from (15) is plotted as black triangles for the wavy latitude with $\theta_0 = \pi/4$ and “amplitude” A ranging from 0 to 0.3. Also plotted is the analogous term from $\mathcal{N} = 4$ SYM perturbation theory (red dots). As they are guaranteed to by the results of [28], the data agree excellently.

$$\Sigma_1 = \frac{\hat{\lambda}^2}{4} \int_0^{2\pi} d\tau_1 \int_0^{\tau_1} d\tau_2 \int_0^{\tau_2} d\tau_3 \int_0^{\tau_3} d\tau_4 \left[Q(\tau_1, \tau_4)Q(\tau_2, \tau_3) + Q(\tau_1, \tau_2)Q(\tau_3, \tau_4) \right] \quad (24)$$

where $Q(\tau_1, \tau_2)$ is defined by the integrand in (25). We call this contribution the “two-rung contribution”. At $\mathcal{O}(\lambda)$, there is no need to verify agreement of the wavy latitudes with (15), as this agreement can already be proven for a general contour as explained in the introduction. That being said, we may continue with the one-loop analysis anyways, as it serves as a warm-up to the two-loop analysis which follows. Expanding (1) to leading order in the ’t Hooft coupling λ , we find

$$\langle W \rangle = 1 + \frac{\hat{\lambda}}{4} \int d\tau_1 \int d\tau_2 \frac{(\dot{x}_1 \cdot \dot{x}_2)(x_1 \cdot x_2 - 1) - (x_1 \cdot \dot{x}_2)(x_2 \cdot \dot{x}_1)}{2(1 - x_1 \cdot x_2)} \quad (25)$$

where $x_i = \vec{x}(\tau_i)$, we have used the fact that $x_i^2 = 1$, and we have defined $\hat{\lambda} \equiv \lambda/(4\pi^2)$. It is not particularly illuminating to substitute the expression for the wavy latitude (23) into this expression. Instead we note that for $A < \theta_0$ (at $A = \theta_0$ the contour self-intersects and thus develops cusps) the expression (25) may be integrated numerically to high accuracy. The expectation from (15), requires the evaluation of

$$\mathcal{A}_1 = \int_0^{2\pi} d\tau (1 - \cos(\theta_0 + A \cos n\tau)). \quad (26)$$

This integral also requires numerical integration, however it may be evaluated with extremely high accuracy. In figure 8 we have plotted the coefficients of $\hat{\lambda}$ from expressions (25) and (15) for $\theta_0 = \pi/4$ and the “amplitude” A ranging from 0 to 0.3. The data lie on top of one another, and the error bars lie within the data points⁵.

⁵In these expressions there is no dependence on n .

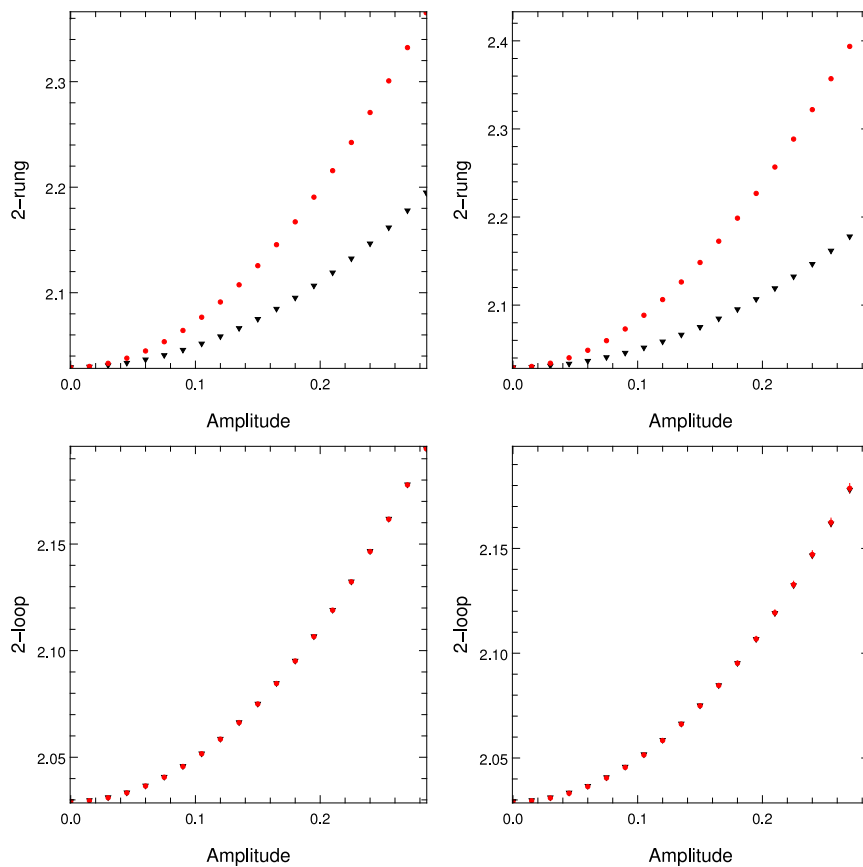


Figure 9: In the top two graphs, the “two-rung” contribution $\Sigma_1/\hat{\lambda}^2$ (see (24)) is plotted as red dots for the contours (23) with $\theta_0 = \pi/4$, “amplitude” A ranging from 0 to 0.3, and for $n = 2$ on the left and $n = 3$ on the right. Also plotted, as black triangles, is the expectation from (15). In the bottom two graphs, we have replaced $\Sigma_1 \rightarrow \Sigma_1 + \Sigma_2 + \Sigma_3$, i.e. the full two-loop result; the agreement with (15) is excellent.

In figure 9 we show the numerical evaluation of the two-rung contribution (see (24)) $\Sigma_1/\hat{\lambda}^2$ for $\theta_0 = \pi/4$, A ranging from 0 to 0.3, and for $n = 2, 3$. Also plotted is the coefficient of $\hat{\lambda}^2$ expected from (15). It is clear that the two-rung diagram alone does not agree with (15), except in the trivial case $A = 0$ when the regular latitude is recovered. Also in figure 9, in the bottom two graphs, we show the same analysis, however this time adding the contribution from $\Sigma_2 + \Sigma_3$ (see (13)). It is seen that within numerical accuracy, which is excellent, there is agreement with the expectation from (15).

2.3 Comments on numerical accuracy

The mechanism whereby the divergence present in (13) cancels was discussed in [20]. The divergence is found by setting the Feynman parameter γ to zero. One then finds⁶

$$(\Sigma_2 + \Sigma_3)_{\gamma=0} = -\frac{\lambda^2}{4} \int_0^1 \frac{d\alpha}{\alpha(1-\alpha)} \oint d\tau_1 d\tau_2 d\tau_3 \epsilon(\tau_1 \tau_2 \tau_3) (\partial_{\tau_2} + \partial_{\tau_1}) \left(\frac{D(\tau_1, \tau_3)}{(x_1 - x_2)^2} \right) \quad (27)$$

where the derivative in τ_2 comes from the first term in (13) and the derivative in τ_1 from the second. Migrating these derivatives to the path ordering symbol via integration by parts, equal and opposite factors of $\delta(\tau_1 - \tau_2)$ are obtained. Thus in the τ_1 - τ_2 integration there are logarithmic divergences which cancel between the first and second term. By exploiting the symmetries of the integration in (13) one can express the integrand such that it is manifestly zero for the case of the 1/2 BPS circle. When a small deformation such as the amplitude A for the wavy latitude is turned on, the compensating logarithmic divergences just described become present, but are weighted by a small number which doesn't compete with the rest of the integral. For a large enough deformation however, the weighting is competitive and the error stemming from the numerical integration's inability to reliably cancel-out non-converging regions becomes significant. Although slightly modified due to its piecewise definition, the same comments apply to the case of the two longitudes. This is why we have been unable to obtain reliable results when δ is near zero. Analyzing the wavy latitudes for larger n or A similarly leads to poor convergence.

3 Connected correlator

At a given order in perturbation theory, it is generally simpler to calculate a connected correlator of two Wilson loops as compared to the VEV of a single loop. This fact was exploited for the 1/2 BPS circle in [4, 5] to check the matrix model conjecture [9, 10] to third order in the 't Hooft coupling. We have therefore computed the connected correlator of two Wilson loops of the variety (1), given by two distinct latitudes at polar angles θ_0^1, θ_0^2 on S^2 , see figure 10. The result is compared, in the limit that the latitudes are coincident, with the computation performed using the reduced 2-d model in light-cone gauge, where there are only ladder diagrams. The latter result is proportional to h^2 , where $h = \cos \theta_0^1 - \cos \theta_0^2$. Unfortunately we are only able to calculate the SYM result at $\mathcal{O}(h^0)$, where we find zero. This leaves open the possibility of further cancellations down to $\mathcal{O}(h^2)$, where a match to the 2-d theory might indeed be found.

As discussed in the introduction, the reduced 2-d model light-cone gauge propagator joining the two latitudes has the following structure

$$D_{2d} = D_{4d} + iD_0 \quad (28)$$

⁶The divergent α integral represents an integrable singularity for the other Feynman parameter β .

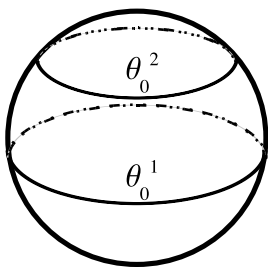
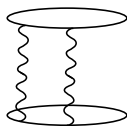
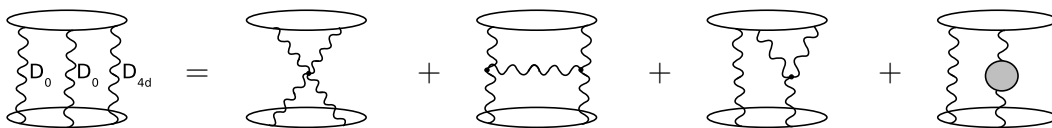


Figure 10: Two distinct Wilson loops given by latitudes at polar angles θ_0^1 and θ_0^2 .

where D_{4d} is the combined gauge and scalar field propagator joining the latitudes in $\mathcal{N} = 4$ supersymmetric Yang-Mills theory in four dimensions, while D_0 is an extra piece (here proportional to the difference in polar angles, i.e. h). Working with gauge group $SU(N)$, and in the large- N limit, it is trivial to show equivalence between the connected correlator in the 2-d and 4-d theories at order λ^2 . This is because in both cases, only the 2-rung ladder diagram



contributes. Because of the form of D_0 , it is then straight-forward to see that its presence integrates to zero. The real test comes at the next order in the 't Hooft coupling. At this level one can show that, should the reduced 2-d model capture the physics



where, on the LHS we have a contribution which stems from a 2-d model diagram with three propagators, however with two insertions of the imaginary part of the propagator (i.e. D_0), and on the RHS we have a sum of interacting diagrams of the 4-d theory, $\mathcal{N} = 4$ SYM, and where all possible variants including scalar fields are implied. The LHS contribution may be obtained precisely, as the integrals over the points on the latitudes are evaluable. On the RHS we find a by now well-known divergence cancellation between the last two diagrams. We can then express everything in terms of finite integrals over the bulk space-time interaction points. These in turn can be analyzed in the limit where the two latitudes are coincident. The results are that



while,

$$\sim |h|^2.$$

3.1 Preliminaries

The latitudes we consider are given by

$$W = \frac{1}{N} \text{Tr} \mathcal{P} \exp \oint d\tau (i \dot{x}^\mu A_\mu + |\dot{x}| \Theta^I \Phi_I), \quad (29)$$

where

$$x^\mu = (s\theta_0 \cos \tau, s\theta_0 \sin \tau, c\theta_0), \quad \Theta^I = (-c\theta_0 \cos \tau, -c\theta_0 \sin \tau, s\theta_0), \quad (30)$$

and where we have used the shorthand $c\theta_0 \equiv \cos \theta_0$ and similarly for sin. The combined gauge field and scalar propagator joining the two latitudes (in Feynman gauge) is then given by

$$D_{12} \equiv \frac{g^2}{4\pi^2} \frac{-\dot{x}_1 \cdot \dot{x}_2 + |\dot{x}_1| |\dot{x}_2| \Theta_1 \cdot \Theta_2}{(x_1 - x_2)^2} = \frac{g^2}{4\pi^2} \frac{s\theta_0^1 s\theta_0^2 [\cos \tau_{12} (c\theta_0^1 c\theta_0^2 - 1) + s\theta_0^1 s\theta_0^2]}{2(1 - c\theta_0^1 c\theta_0^2 - s\theta_0^1 s\theta_0^2 \cos \tau_{12})}. \quad (31)$$

This ‘‘loop-to-loop propagator’’ is more compactly expressed as

$$D_{12} = \frac{g^2}{4\pi^2} \frac{(1 - c\theta_0^1 c\theta_0^2)}{2} \left(\frac{\cos \tau_{12} + \Lambda}{\cos \tau_{12} + \Lambda^{-1}} \right), \quad \Lambda \equiv \frac{s\theta_0^1 s\theta_0^2}{c\theta_0^1 c\theta_0^2 - 1}. \quad (32)$$

We are interested also in a reduced 2-d theory living on an S^2 parametrized by the complex variable z such that

$$x^\mu = \frac{1}{1 + z\bar{z}} (z + \bar{z}, -i(z - \bar{z}), 1 - z\bar{z}) \quad (33)$$

and so $z = e^{i\tau} \tan(\theta_0/2)$ describes our latitudes. This theory is pure gauge. Its fields are A_z and $A_{\bar{z}}$. In the light-cone gauge $A_{\bar{z}} = 0$ while [28, 29]

$$\langle A_z(z) A_z(w) \rangle = \frac{2g_{2d}^2}{\pi} \frac{1}{(1 + z\bar{z})} \frac{1}{(1 + w\bar{w})} \frac{\bar{z} - \bar{w}}{z - w}, \quad (34)$$

where $g_{2d}^2 = -g^2/(4\pi)$. In this theory we may also construct the standard Wilson loop $\frac{1}{N} \text{Tr} \mathcal{P} \exp i \oint A dx$. The loop-to-loop propagator here is

$$\mathcal{D}_{12} = i^2 \dot{z}_1 \dot{z}_2 \langle A_z(z_1) A_z(z_2) \rangle = \frac{2g_{2d}^2}{\pi} \frac{s\theta_0^1 s\theta_0^2}{4} \left(\frac{\lambda_1^2 e^{-i\tau_{12}} + \lambda_2^2 e^{i\tau_{12}} - 2\lambda_1 \lambda_2}{\lambda_1^2 + \lambda_2^2 - 2\lambda_1 \lambda_2 \cos \tau_{12}} \right) \quad (35)$$

where $\lambda_i = \tan(\theta_0^i/2)$. This can be put into a much more suggestive form



Figure 11: These 2-d theory diagrams are trivially equivalent to their 4-d counterparts.

$$\mathcal{D}_{12} = \frac{g^2}{4\pi^2} \frac{(1 - c\theta_0^1 c\theta_0^2)}{2} \left(\frac{\cos \tau_{12} + \Lambda}{\cos \tau_{12} + \Lambda^{-1}} \right) + i \frac{g^2}{4\pi^2} \frac{(c\theta_0^1 - c\theta_0^2)}{2} \left(\frac{\sin \tau_{12}}{\cos \tau_{12} + \Lambda^{-1}} \right) \quad (36)$$

where we see that the real component is exactly the loop-to-loop propagator in the 4-d theory, i.e. D_{12} defined in (31).

3.2 A relation between diagrams

We are interested in calculating the connected correlator between two Wilson lattitudes, both in the 2-d and 4-d theory. We begin with the 2-d calculation. We perform calculations using the gauge group $SU(N)$, in the large N limit. Therefore we are interested only in planar diagrams, while single insertions on a Wilson loop vanish since the generators of $SU(N)$ are traceless. The 2-d theory, being in the light-cone gauge, is free of interactions - it has only ladder diagrams. In fact there are three 2-d ladder diagrams which are trivially equivalent to those of the 4-d theory. These are pictured in figure 11. In the first two diagrams, due to the fact that at least one of the loops has only two insertions, and due to the cyclicity of the trace, the imaginary component of (36) integrates to zero since

$$\int_0^{2\pi} d\theta \frac{\sin \theta}{\cos \theta + \Lambda^{-1}} = 0. \quad (37)$$

Similarly, in the last diagram, any insertions of the imaginary component of the loop-to-loop propagator vanish. Therefore only the real component of the propagator contributes - giving precisely the result for the 4-d theory. At order λ^2 the only non-vanishing planar diagram in either theory is the two-rung ladder (pictured in figure 11 for the 2-d theory). Thus the two theories agree at this level, however this is a direct result of the one-loop proof given in [28, 29].

Up to order λ^3 there is only one other planar ladder diagram - the triple rung. The triple rung is given by

$$\begin{aligned} \text{Triple Rung Diagram} &= \frac{N^3}{8N^2} \int_0^{2\pi} d\tau_1 \int_0^{\tau_1} d\tau_2 \int_0^{\tau_2} d\tau_3 \int_0^{2\pi} d\sigma_1 \int_0^{\sigma_1} d\sigma_2 \int_0^{\sigma_2} d\sigma_3 \left\{ \mathcal{D}_{\sigma_1 \tau_1} \mathcal{D}_{\sigma_2 \tau_2} \mathcal{D}_{\sigma_3 \tau_3} \right. \\ &\quad \left. + \mathcal{D}_{\sigma_1 \tau_3} \mathcal{D}_{\sigma_2 \tau_1} \mathcal{D}_{\sigma_3 \tau_2} + \mathcal{D}_{\sigma_1 \tau_2} \mathcal{D}_{\sigma_2 \tau_3} \mathcal{D}_{\sigma_3 \tau_1} \right\}. \end{aligned}$$

Upon substitution of the 2-d theory propagator (36), we see that the terms involving an odd number of insertions of the imaginary component vanish, whereas clearly three insertions of the real component gives exactly the triple rung in the 4-d theory. We are therefore left with the following equality, should the 2-d theory truly agree with the 4-d

$$\begin{aligned}
\text{III} &= \frac{\pi}{12N^2} \left(\frac{g^2 N}{8\pi^2} \right)^3 i^2 (c\theta_0^1 - c\theta_0^2)^2 (1 - c\theta_0^1 c\theta_0^2) \int_0^{2\pi} d\phi \int_0^{2\pi} d\theta_1 \int_0^{2\pi} d\theta_2 \int_0^{\theta_1} d\psi_1 \int_0^{\theta_2} d\psi_2 \\
&\left\{ \left(\frac{\cos(\phi + \theta_2) + \Lambda}{\cos(\phi + \theta_2) + \Lambda^{-1}} \right) \left(\frac{\sin(\phi + \psi_2 - \theta_1)}{\cos(\phi + \psi_2 - \theta_1) + \Lambda^{-1}} \right) \left(\frac{\sin(\phi - \psi_1)}{\cos(\phi - \psi_1) + \Lambda^{-1}} \right) \right. \\
&+ \left(\frac{\sin(\phi + \theta_2)}{\cos(\phi + \theta_2) + \Lambda^{-1}} \right) \left(\frac{\cos(\phi + \psi_2 - \theta_1) + \Lambda}{\cos(\phi + \psi_2 - \theta_1) + \Lambda^{-1}} \right) \left(\frac{\sin(\phi - \psi_1)}{\cos(\phi - \psi_1) + \Lambda^{-1}} \right) \\
&+ \left. \left(\frac{\sin(\phi + \theta_2)}{\cos(\phi + \theta_2) + \Lambda^{-1}} \right) \left(\frac{\sin(\phi + \psi_2 - \theta_1)}{\cos(\phi + \psi_2 - \theta_1) + \Lambda^{-1}} \right) \left(\frac{\cos(\phi - \psi_1) + \Lambda}{\cos(\phi - \psi_1) + \Lambda^{-1}} \right) \right\} \\
&= \text{Sum of interacting diagrams of 4-d theory: X, H, IY, and 2-rung bubble}
\end{aligned} \tag{38}$$

i.e., the triple-rung with two insertions of the imaginary component of the loop-to-loop propagator ought to equal the sum of all remaining diagrams of the 4-d theory - the so-called X, H, IY, and 1-loop corrected two-rung ladder (or “2-rung bubble”) diagrams. We visit these diagrams individually in appendix B; they are depicted in figure 15.

The integrations in (38) can be carried out rather simply because of the happy fact that

$$\frac{\sin \phi}{\cos \phi + \Lambda^{-1}} = -\partial_\phi \ln(-\Lambda^{-1} - \cos \phi) \tag{39}$$

where we have ensured that the argument of the \ln is always positive. The result is⁷

$$\begin{aligned}
\text{III} &= \frac{\pi}{4N^2} \left(\frac{g^2 N}{8\pi^2} \right)^3 i^2 (c\theta_0^1 - c\theta_0^2)^2 \left(1 - c\theta_0^1 c\theta_0^2 - |c\theta_0^1 - c\theta_0^2| \right) (2\pi)^3 \\
&\times \left[-2 \text{Li}_2 \left(\frac{r^2 - 1}{r^2} \right) + 2 \ln r^2 \ln \frac{r^2 - 1}{r^2} + \frac{\pi^2}{3} \right]
\end{aligned} \tag{40}$$

where

$$r \equiv \frac{1 - c\theta_0^1 c\theta_0^2 + |c\theta_0^1 - c\theta_0^2|}{s\theta_0^1 s\theta_0^2}, \quad r^{-1} = \frac{1 - c\theta_0^1 c\theta_0^2 - |c\theta_0^1 - c\theta_0^2|}{s\theta_0^1 s\theta_0^2}, \quad \Lambda^{-1} = -\frac{1}{2}(r + r^{-1}). \tag{41}$$

⁷In an earlier version of this manuscript an error was present in (40) giving a mismatch with zero-instanton QCD₂.

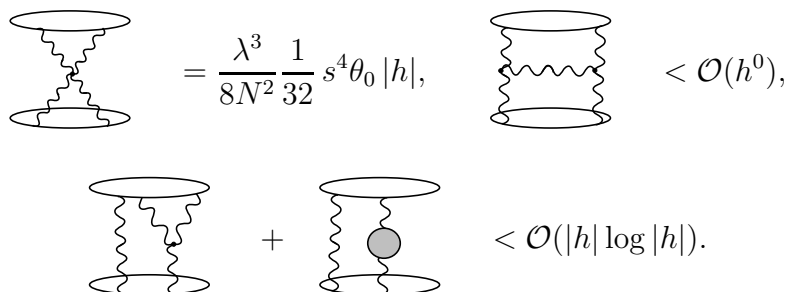
We are therefore interested in whether or not this expression can be recovered by the sum of interacting diagrams of the 4-d theory.

3.3 Results

We will investigate the proposed relation (38) in the limit in which the two latitudes are coincident. Looking at (40) we see that in this limit (where $r \rightarrow 1$)

$$\text{III} \simeq -\frac{\lambda^3}{N^2} \frac{s^2 \theta_0}{2^8 \cdot 3} (c\theta_0^1 - c\theta_0^2)^2 \sim |h|^2. \quad (42)$$

The evaluation of the X, H, and IY diagrams are collected in appendix B. The results in the coincident limit $\theta_0^1 \simeq \theta_0^2 \simeq \theta_0$ are as follows



$$\begin{aligned}
 & \text{Diagram 1} = \frac{\lambda^3}{8N^2} \frac{1}{32} s^4 \theta_0 |h|, \quad \text{Diagram 2} < \mathcal{O}(h^0), \\
 & \text{Diagram 3} + \text{Diagram 4} < \mathcal{O}(|h| \log |h|).
 \end{aligned}$$

4 Discussion

The stunning agreement found in section 2 for the VEV of a single Wilson loop at $\mathcal{O}(\lambda^2)$ is the result of an intriguing cancellation of interacting Feynman diagrams with rainbow/ladders. It certainly points to the capturing of these loops by a reduced model, which for single Wilson loop VEV's agrees with the proposal made in [29], while for Wilson loop correlators, does not disagree. It remains a challenge to push the SYM correlator calculation to further orders in h , or ideally, to an exact result which could be matched against the 2-d model.

There are also further analyses which could be carried out. One of these is to consider the connected correlator in the limit as one of the latitudes shrinks to a point. A similar limit was taken in the work [5], for two 1/2 BPS circles. There it was shown that the shrunken Wilson loop is given by a sum of local operators, both protected and unprotected by supersymmetry. The unprotected operators lead to terms which diverge as the logarithm of the radius of the shrinking loop; these logarithms arise from the interacting graphs and allow the determination of the operator's anomalous dimension at first order in the 't Hooft coupling. It would be interesting to repeat this analysis using the results collected here; we leave this to a further publication. It would also be interesting to compute the connected correlator at strong coupling, using string theory; there two-point functions with protected operators may be accessible [19–22]. If so, the summation of ladder diagrams along the lines of [20, 22] could be attempted in the gauge theory and compared.

Acknowledgements

It is a pleasure to thank Jan Plefka and Matthias Staudacher for discussions, and Nadav Drukker for discussions and for suggesting these calculations. The author would also like to thank the Galileo Galilei Institute for Theoretical Physics for hospitality during the later stages of completion of this work. This work was funded in part by a Postdoctoral Fellowship from the Natural Sciences and Engineering Research Council of Canada (NSERC), and also by the Volkswagen Foundation.

A Longitudes: divergence cancellation

It is known that the two-loop diagrams with internal vertices cancel-out for the 1/2 BPS circle. However, here, in the case of two longitudes, we will not find the same cancellation. We find a finite remainder, which is zero in the $\delta = \pi$ limit. To begin, we re-cap the cancellation mechanism for the 1/2 BPS circle. Equation (28) of [9] gives the contribution from the triple vertex diagram as

$$\begin{aligned} \Sigma_3 = & \lambda^2 \frac{\Gamma(2\omega - 2)}{2^{2\omega+5} \pi^{2\omega}} \int_0^1 d\alpha d\beta d\gamma (\alpha\beta\gamma)^{\omega-2} \delta(1 - \alpha - \beta - \gamma) \\ & \times \oint d\tau_1 d\tau_2 d\tau_3 \frac{\epsilon(\tau_1 \tau_2 \tau_3)(1 - \cos \tau_{13})(\alpha(1 - \alpha) \sin \tau_{12} + \alpha\gamma \sin \tau_{23})}{[\alpha\beta(1 - \cos \tau_{12}) + \beta\gamma(1 - \cos \tau_{23}) + \gamma\alpha(1 - \cos \tau_{13})]^{2\omega-2}}. \end{aligned} \quad (43)$$

By using the identity

$$\oint d\tau_1 d\tau_2 d\tau_3 \frac{\partial}{\partial \tau_1} \frac{\epsilon(\tau_1 \tau_2 \tau_3)(1 - \cos \tau_{13})}{\Delta^{2\omega-3}} = 0 \quad (44)$$

where $\Delta = \alpha\beta(1 - \cos \tau_{12}) + \beta\gamma(1 - \cos \tau_{23}) + \gamma\alpha(1 - \cos \tau_{13})$, and $\omega = 2$ on the physical dimension, one may relate Σ_3 to the one-loop-corrected, single-rung ladder diagram, and an extra piece which vanishes on the physical dimension.

A.1 Insertions on a single longitude

The simplest class of triple vertex diagrams for the two longitudes are pictured in figure 12.

We can use (43) for these diagrams as well, the only difference being the range of the loop parameters, which invalidates (44). This means that after the cancellation of the self-energy diagrams shown schematically in figure 12, there is a finite quantity left-over. If we take the range of the τ_i to be between 0 and π , then we have that the RHS of (44) is no longer zero but (under integration over α, β, γ)

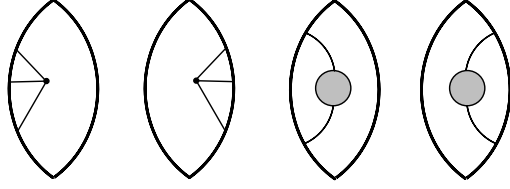


Figure 12: Simplest class of triple vertex diagrams for the two longitudes. The solid lines refer to both scalars and gauge fields.

$$\int_0^\pi d\tau_2 \int_0^{\tau_2} d\tau_3 \left\{ \frac{\cos \tau_3 - \cos \tau_2}{[\alpha\beta(1 + \cos \tau_2) + \beta\gamma(1 - \cos \tau_{23}) + \gamma\alpha(1 + \cos \tau_3)]^{2\omega-3}} + \frac{\cos \tau_3 - \cos \tau_2}{[\alpha\beta(1 - \cos \tau_2) + \beta\gamma(1 - \cos \tau_{23}) + \gamma\alpha(1 - \cos \tau_3)]^{2\omega-3}} \right\} \quad (45)$$

The complement of this contribution, where the loop parameters travel between π and 2π , is

$$\int_\pi^{2\pi} d\tau_2 \int_\pi^{\tau_2} d\tau_3 \left\{ \frac{-\cos \tau_3 + \cos \tau_2}{[\alpha\beta(1 - \cos \tau_2) + \beta\gamma(1 - \cos \tau_{23}) + \gamma\alpha(1 - \cos \tau_3)]^{2\omega-3}} + \frac{-\cos \tau_3 + \cos \tau_2}{[\alpha\beta(1 + \cos \tau_2) + \beta\gamma(1 - \cos \tau_{23}) + \gamma\alpha(1 + \cos \tau_3)]^{2\omega-3}} \right\} \quad (46)$$

By shifting the loop parameters by π in (46) we find that it is just equal to (45). We will see that these quantities are removed when we consider insertions between the two longitudes.

A.2 Insertions between the two longitudes

The next class of triple vertex diagrams are those that connect the two longitudes. In figure 13 we have shown those with two insertions on the $0 \rightarrow \pi$ contour, however we must equally consider those with two insertions on the opposite contour. These diagrams can essentially be “read-off” from (43). The results are

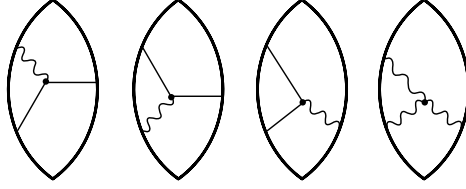


Figure 13: Triple vertex diagrams which connect two longitudes. These diagrams do not cancel completely against the diagram shown in figure 14.

$$\begin{aligned}
\Sigma_3 = & \frac{\lambda^2}{4} \int_{\pi}^{2\pi} d\tau_1 \int_0^{\pi} d\tau_2 \int_0^{\pi} d\tau_3 \epsilon(\tau_2 \tau_3) \left\{ (\dot{y}_1 \cdot \dot{x}_2 + \cos \delta) \dot{x}_3 \cdot (\partial_{x_2} - \partial_{y_1}) \right. \\
& \left. + (\dot{x}_2 \cdot \dot{x}_3 - 1) \dot{y}_1 \cdot \partial_{x_3} \right\} G(y_1, x_2, x_3) \\
& - \frac{\lambda^2}{4} \int_{\pi}^{2\pi} d\tau_1 \int_{\pi}^{2\pi} d\tau_2 \int_0^{\pi} d\tau_3 \epsilon(\tau_1 \tau_2) \left\{ (\dot{y}_2 \cdot \dot{x}_3 + \cos \delta) \dot{y}_1 \cdot (\partial_{y_2} - \partial_{x_3}) \right. \\
& \left. + (\dot{y}_1 \cdot \dot{y}_2 - 1) \dot{x}_3 \cdot \partial_{y_1} \right\} G(y_1, y_2, x_3)
\end{aligned} \tag{47}$$

where

$$\begin{aligned}
G(y_1, x_2, x_3) &= \frac{\Gamma(2\omega - 3)}{2^{2\omega+3}\pi^{2\omega}} \int_0^1 d\alpha d\beta d\gamma (\alpha\beta\gamma)^{\omega-2} \delta(1 - \alpha - \beta - \gamma) \frac{1}{\Delta^{2\omega-3}}, \\
G(y_1, y_2, x_3) &= \frac{\Gamma(2\omega - 3)}{2^{2\omega+3}\pi^{2\omega}} \int_0^1 d\alpha d\beta d\gamma (\alpha\beta\gamma)^{\omega-2} \delta(1 - \alpha - \beta - \gamma) \frac{1}{\tilde{\Delta}^{2\omega-3}}
\end{aligned}$$

where

$$\begin{aligned}
\Delta &= \alpha\beta(1 + \sigma \sin \tau_1 \sin \tau_2 - \cos \tau_1 \cos \tau_2) \\
&+ \beta\gamma(1 - \cos \tau_{23}) + \alpha\gamma(1 + \sigma \sin \tau_1 \sin \tau_3 - \cos \tau_1 \cos \tau_3) \\
\tilde{\Delta} &= \alpha\beta(1 - \cos \tau_{12}) + \beta\gamma(1 + \sigma \sin \tau_2 \sin \tau_3 - \cos \tau_2 \cos \tau_3) \\
&+ \alpha\gamma(1 + \sigma \sin \tau_1 \sin \tau_3 - \cos \tau_1 \cos \tau_3)
\end{aligned} \tag{48}$$

and where $\sigma \equiv \cos \delta$. In fact the second expression is just equal to the first, and so we are free to take twice the first expression.

Our strategy will be to generalize the mechanism used for the 1/2 BPS circle, described under equation (44), to the present case. We will be looking to cancel out the divergent diagram shown in figure 14. This diagram gives the following contribution (see equation (12) of [9])

$$- \frac{\lambda^2 \Gamma^2(\omega - 1)}{128\pi^{2\omega}(2 - \omega)(2\omega - 3)} 2 \int_{\pi}^{2\pi} dt_1 \int_0^{\pi} dt_2 \frac{\cos \delta \cos t_1 \cos t_2 - \sin t_1 \sin t_2 - \cos \delta}{[2(1 + \cos \delta \sin t_1 \sin t_2 - \cos t_1 \cos t_2)]^{2\omega-3}}. \tag{49}$$

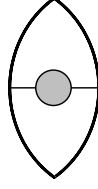


Figure 14: The one-loop-corrected one rung ladder; it is divergent and must be cancelled by the diagrams shown in figure 13.

Therefore we will consider

$$\begin{aligned}
& \partial_{\tau_3} \frac{(\sigma \cos \tau_1 \cos \tau_3 - \sigma - \sin \tau_1 \sin \tau_3)}{\Delta^{2\omega-3}} \\
&= \frac{(2\omega - 3)}{\Delta^{2\omega-2}} \left[\sigma \cos \tau_1 \cos \tau_3 - \sigma - \sin \tau_1 \sin \tau_3 \right] \left[\beta \gamma \sin \tau_{23} - \alpha \gamma (\sigma \sin \tau_1 \cos \tau_3 + \cos \tau_1 \sin \tau_3) \right] \\
&+ \frac{1}{\Delta^{2\omega-2}} \left[\Delta \right] \left[-\sin \tau_1 \cos \tau_3 - \sigma \cos \tau_1 \sin \tau_3 \right]
\end{aligned} \tag{50}$$

where $\Delta = \alpha\beta(1 + \sigma \sin \tau_1 \sin \tau_2 - \cos \tau_1 \cos \tau_2) + \beta\gamma(1 - \cos \tau_{23}) + \alpha\gamma(1 + \sigma \sin \tau_1 \sin \tau_3 - \cos \tau_1 \cos \tau_3)$. The first contribution from the integrand in (47) is

$$\begin{aligned}
A_1 &= (\dot{y}_1 \cdot \dot{x}_2 + \sigma) \dot{x}_3 \cdot \partial_{x_2} \frac{1}{\Delta^{2\omega-3}} = (3 - 2\omega) \left[\sigma(1 - \cos \tau_1 \cos \tau_2) + \sin \tau_1 \sin \tau_2 \right] \\
&\quad \times \left[\beta(\alpha + \gamma) \sin \tau_{23} + \alpha\beta (\sigma \sin \tau_1 \cos \tau_3 + \cos \tau_1 \sin \tau_3) \right] \frac{1}{\Delta^{2\omega-2}}.
\end{aligned} \tag{51}$$

We use (50) to derive the following relation

$$\begin{aligned}
& \mathcal{N} \int_{\pi}^{2\pi} d\tau_1 \int_0^{\pi} d\tau_2 \int_0^{\pi} d\tau_3 \epsilon(\tau_2 \tau_3) A_1 \\
&= \mathcal{N}(3 - 2\omega) \left[\int_{\pi}^{2\pi} d\tau_1 \int_0^{\pi} d\tau_2 \frac{-\sigma - \sigma c_1}{\Delta^{2\omega-3}|_{\tau_3=\pi}} - \int_{\pi}^{2\pi} d\tau_1 \int_0^{\pi} d\tau_2 \frac{\sigma - \sigma c_1}{\Delta^{2\omega-3}|_{\tau_3=0}} \right] \\
&\quad + \mathcal{N}(3 - 2\omega) \int_{\pi}^{2\pi} d\tau_1 \int_0^{\pi} d\tau_2 \int_0^{\pi} d\tau_3 \epsilon(\tau_2 \tau_3) \frac{B_1}{\Delta^{2\omega-2}} \\
&\quad - 2\lambda^2 \frac{\Gamma(2\omega - 3) \Gamma^2(\omega - 1) \Gamma(2 - \omega)}{2^{2\omega+3} \pi^{2\omega} \Gamma(2\omega - 2) \Gamma(5 - \omega)} \int_{\pi}^{2\pi} d\tau_1 \int_0^{\pi} d\tau_2 \frac{\sigma - \sigma c_1 c_2 + s_1 s_2}{[(1 + \sigma s_1 s_1 - c_1 c_2)]^{2\omega-3}}
\end{aligned} \tag{52}$$

where $c_i \equiv \cos \tau_i$, $s_i \equiv \sin \tau_i$, finite terms multiplied by $(2\omega - 4)$ have been suppressed, B_1 is given along with similar contributions from the other portions of the integrand in (47) in (61), and we have introduced the notation

$$\mathcal{N} \equiv \frac{\lambda^2 \Gamma(2\omega - 3)}{2^{2\omega+3} \pi^{2\omega}} \int_0^1 d\alpha d\beta d\gamma \delta(1 - \alpha - \beta - \gamma) (\alpha\beta\gamma)^{\omega-2}. \quad (53)$$

In the limit $\omega \rightarrow 2$ the singular contribution in the last line of (52) cancels (49) exactly. The first two terms represent finite quantities left over from this cancellation. We may now continue and derive similar identities for the remaining terms in (47). Continuing with the second term in the first integral of (47)

$$A_2 = -(\dot{y}_1 \cdot \dot{x}_2 + \sigma) \dot{x}_3 \cdot \partial_{y_1} \frac{1}{\Delta^{2\omega-3}} = (3 - 2\omega) \left[\sigma(1 - \cos \tau_1 \cos \tau_2) + \sin \tau_1 \sin \tau_2 \right] \\ \times \left[\alpha\beta \sin \tau_{23} + \alpha(\beta + \gamma) (\sigma \sin \tau_1 \cos \tau_3 + \cos \tau_1 \sin \tau_3) \right] \frac{1}{\Delta^{2\omega-2}} \quad (54)$$

we use the derivative

$$-\partial_{\tau_3} \frac{(1 - \cos \tau_{23})}{\Delta^{2\omega-3}} = -\frac{(2\omega - 3)}{\Delta^{2\omega-2}} \left[1 - \cos \tau_{23} \right] \left[\beta\gamma \sin \tau_{23} - \alpha\gamma(\sigma \sin \tau_1 \cos \tau_3 + \cos \tau_1 \sin \tau_3) \right] \\ + \frac{1}{\Delta^{2\omega-2}} \left[\Delta \right] \left[\sin \tau_{23} \right] \quad (55)$$

to derive

$$\mathcal{N} \int_{\pi}^{2\pi} d\tau_1 \int_0^{\pi} d\tau_2 \int_0^{\pi} d\tau_3 \epsilon(\tau_2 \tau_3) A_2 \\ = \mathcal{N}(3 - 2\omega) \int_{\pi}^{2\pi} d\tau_1 \int_0^{\pi} d\tau_2 \int_0^{\pi} d\tau_3 \epsilon(\tau_2 \tau_3) \frac{B_2}{\Delta^{2\omega-2}} \\ + \mathcal{N}(3 - 2\omega) \left[\int_{\pi}^{2\pi} d\tau_1 \int_0^{\pi} d\tau_2 \frac{-(1 + c_2)}{\Delta^{2\omega-3}|_{\tau_3=\pi}} - \int_{\pi}^{2\pi} d\tau_1 \int_0^{\pi} d\tau_2 \frac{1 - c_2}{\Delta^{2\omega-3}|_{\tau_3=0}} \right]. \quad (56)$$

Similarly for the third term in (47), we have

$$A_3 = (\dot{x}_2 \cdot \dot{x}_3 - 1) \dot{y}_1 \cdot \partial_{x_3} \frac{1}{\Delta^{2\omega-3}} = (3 - 2\omega) \left[\cos \tau_{23} - 1 \right] \\ \times \left[\beta\gamma (\sigma \cos \tau_1 \sin \tau_2 + \sin \tau_1 \cos \tau_2) - \gamma(\alpha + \beta) (\sigma \cos \tau_1 \sin \tau_3 + \sin \tau_1 \cos \tau_3) \right] \frac{1}{\Delta^{2\omega-2}} \quad (57)$$

and we use the derivative

$$\begin{aligned}
& -\partial_{\tau_1} \frac{(1 - \cos \tau_{13})}{\Delta^{2\omega-3}} \\
& = \frac{(2\omega - 3)}{\Delta^{2\omega-2}} [1 - \cos \tau_{13}] \left[\alpha\beta(\sigma \cos \tau_1 \sin \tau_2 + \sin \tau_1 \cos \tau_2) + \alpha\gamma(\sigma \cos \tau_1 \sin \tau_3 + \sin \tau_1 \cos \tau_3) \right] \\
& + \frac{1}{\Delta^{2\omega-2}} [\Delta] [-\sin \tau_{13}].
\end{aligned} \tag{58}$$

We find

$$\begin{aligned}
\mathcal{N} & \int_{\pi}^{2\pi} d\tau_1 \int_0^{\pi} d\tau_2 \int_0^{\pi} d\tau_3 \epsilon(\tau_2 \tau_3) A_3 \\
& = \mathcal{N}(3 - 2\omega) \int_{\pi}^{2\pi} d\tau_1 \int_0^{\pi} d\tau_2 \int_0^{\pi} d\tau_3 \epsilon(\tau_2 \tau_3) \frac{B_3}{\Delta^{2\omega-2}} \\
& + \mathcal{N}(3 - 2\omega) \left[\int_0^{\pi} d\tau_2 \int_0^{\pi} d\tau_3 \epsilon(\tau_2 \tau_3) \frac{(1 - c_3)}{\Delta^{2\omega-3}|_{\tau_3=2\pi}} - \int_0^{\pi} d\tau_2 \int_0^{\pi} d\tau_3 \epsilon(\tau_2 \tau_3) \frac{(1 + c_3)}{\Delta^{2\omega-3}|_{\tau_3=\pi}} \right].
\end{aligned} \tag{59}$$

The last line above cancels the contributions of (45) and (46) exactly. We are now in a position to quote the finite result of the internal vertex diagrams, it is given by

$$\begin{aligned}
\Lambda_3 = & -\frac{\hat{\lambda}^2}{16} \int_0^1 d\alpha d\beta d\gamma \delta(1 - \alpha - \beta - \gamma) \left[\int_{\pi}^{2\pi} d\tau_1 \int_0^{\pi} d\tau_2 \int_0^{\pi} d\tau_3 \epsilon(\tau_2 \tau_3) \frac{B_1 + B_2 + B_3}{\Delta^2} \right. \\
& \left. - \int_{\pi}^{2\pi} d\tau_1 \int_0^{\pi} d\tau_2 \frac{(1 + \sigma)(2 + c_1 + c_2)}{[\alpha\beta(1 + \sigma s_1 s_2 - c_1 c_2) + \beta\gamma(1 + c_2) + \alpha\gamma(1 + c_1)]} \right]
\end{aligned} \tag{60}$$

where we have combined the surface terms from (52) and (56). A simple expression for the sum of B_1 , B_2 , and B_3 is given by

$$\begin{aligned}
B_1 + B_2 + B_3 = & \alpha\gamma(\sigma^2 - 1) [2s_1(c_3 - c_2) - s_1 c_1(1 - \cos \tau_{23})] \\
& + \alpha\gamma(\sigma + 1)(s_2 - s_3)(c_3 - c_1) \\
& + \alpha\gamma(\sigma + 1) [\sin \tau_{13}^+ - \sin \tau_{12}^+ + \sin \tau_{23}] \\
& + \alpha\gamma(\sigma + 1) \sin \tau_{23}(1 - \cos \tau_{13}^+) + \beta\gamma(\sigma + 1)c_1 s_3(1 - \cos \tau_{23})
\end{aligned} \tag{61}$$

where we have introduced some shorthand $\tau_{ij} \equiv \tau_i - \tau_j$, $\tau_{ij}^+ \equiv \tau_i + \tau_j$. It is clear that at $\delta = \pi$, where $\sigma = -1$, Λ_3 is explicitly zero, as it must be, in order to coincide with the known results of the 1/2 BPS circle.

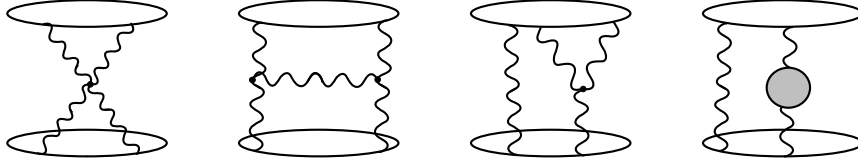


Figure 15: The interacting diagrams of the 4-d theory which contribute to the planar, connected correlator of two Wilson loops. The gauge field lines are understood to also represent scalars - as allowed by the couplings of $\mathcal{N} = 4$ SYM.

B Connected correlator: interacting diagrams

In this section we undertake the calculation of the diagrams depicted⁸ in figure 15, in the 4-d theory, i.e. $\mathcal{N} = 4$ SYM. We employ the Euclidean action in Feynman gauge, the details of which (along with the conventions used here) are to be found in [4] and [9]. We will find that there is a divergence cancellation between the IY and 2-rung bubble, completely analogous to the one found for the case of two 1/2 BPS Wilson circles in [4]. The X and H diagrams will also yield extremely similar - but not exactly the same - results as those found in [4] for the 1/2 BPS case. Due to the great similarity between the following calculation and that performed in [4], we will not be overly explicit. The reader is referred to [4] for further details.

The general strategy is to perform the integrals over the Wilson loop contours themselves, leaving the bulk integrations over the space-time points of interaction unevaluated. We will use the notation $x(\tau)$ and $y(\sigma)$ to refer to the parametrizations of the two Wilson loops at polar angles θ_0^1 and θ_0^2 respectively, along with their associated scalar paths $\Theta_x(\tau)$ and $\Theta_y(\sigma)$. We will find the following integrals repeatedly useful

$$\begin{aligned}
 I(\theta_0) &\equiv \int_0^{2\pi} d\tau \frac{1}{a + b \cos \tau + c \sin \tau} = \frac{2\pi}{\sqrt{a^2 - (b^2 + c^2)}}, \\
 I_c(\theta_0) &\equiv \int_0^{2\pi} d\tau \frac{\cos \tau}{a + b \cos \tau + c \sin \tau} = \frac{2\pi b \left(\sqrt{a^2 - (b^2 + c^2)} - a \right)}{\sqrt{a^2 - (b^2 + c^2)} (b^2 + c^2)}, \\
 I_s(\theta_0) &\equiv \int_0^{2\pi} d\tau \frac{\sin \tau}{a + b \cos \tau + c \sin \tau} = \frac{2\pi c \left(\sqrt{a^2 - (b^2 + c^2)} - a \right)}{\sqrt{a^2 - (b^2 + c^2)} (b^2 + c^2)},
 \end{aligned} \tag{62}$$

where

$$a = \rho^2 + w_3^2 + s^2 \theta_0 + (w_2 - c \theta_0)^2, \quad b = -2 s \theta_0 w_0, \quad c = -2 s \theta_0 w_1, \tag{63}$$

⁸There is also a second IY diagram, where the two latitudes are exchanged.

and $\rho^2 = w_0^2 + w_1^2$, where $w = (w_0, w_1, w_2, w_3)$ is a space-time interaction point. We will also make use of some further shorthand

$$R_1 \equiv \rho^2 + w_2^2 + w_3^2, \quad R_2 \equiv (\rho + \cot \theta_0)^2 + (w_2 - 1)^2 + w_3^2. \quad (64)$$

B.1 X diagram

The X-diagram is given by

$$\begin{aligned} X = & \frac{8g^6 N^3}{4^3 N^2} \int_0^{2\pi} d\tau_1 \int_0^{2\pi} d\tau_2 \int_0^{2\pi} d\sigma_1 \int_0^{2\pi} d\sigma_2 \\ & \left[\left(\dot{x}_1 \cdot \dot{y}_2 - \Theta_{x_1} \cdot \Theta_{y_2} |\dot{x}_1| |\dot{y}_2| \right) \left(\dot{x}_2 \cdot \dot{y}_1 - \Theta_{x_2} \cdot \Theta_{y_1} |\dot{x}_2| |\dot{y}_1| \right) \right. \\ & \left. - \left(\dot{x}_1 \cdot \dot{x}_2 - \Theta_{x_1} \cdot \Theta_{x_2} |\dot{x}_1| |\dot{x}_2| \right) \left(\dot{y}_1 \cdot \dot{y}_2 - \Theta_{y_1} \cdot \Theta_{y_2} |\dot{y}_1| |\dot{y}_2| \right) \right] \\ & \times \left(\frac{1}{4\pi^2} \right)^4 \int \frac{d^4 w}{(x_1 - w)^2 (x_2 - w)^2 (y_1 - w)^2 (y_2 - w)^2} \end{aligned} \quad (65)$$

Evaluating the integrals over $\tau_1, \tau_2, \sigma_1, \sigma_2$, we have

$$\begin{aligned} X = & \frac{8g^6 N^3}{4^3 N^2} \left(\frac{1}{4\pi^2} \right)^4 \int d^4 w \left\{ s^2 \theta_0^1 s^2 \theta_0^2 (1 - c\theta_0^1 c\theta_0^2)^2 \left[I_c(\theta_0^1) I_c(\theta_0^2) + I_s(\theta_0^1) I_s(\theta_0^2) \right]^2 \right. \\ & - 2s^3 \theta_0^1 s^3 \theta_0^2 (1 - c\theta_0^1 c\theta_0^2) I(\theta_0^1) I(\theta_0^2) \left[I_c(\theta_0^1) I_c(\theta_0^2) + I_s(\theta_0^1) I_s(\theta_0^2) \right] \\ & + s^4 \theta_0^1 s^4 \theta_0^2 \left(I^2(\theta_0^2) \left[I_c^2(\theta_0^1) + I_s^2(\theta_0^1) \right] + I^2(\theta_0^1) \left[I_c^2(\theta_0^2) + I_s^2(\theta_0^2) \right] \right) \\ & \left. - s^4 \theta_0^1 s^4 \theta_0^2 \left(I_c^2(\theta_0^1) + I_s^2(\theta_0^1) \right) \left(I_c^2(\theta_0^2) + I_s^2(\theta_0^2) \right) \right\} \end{aligned} \quad (66)$$

where the I, I_c, I_s are given by (62), (63).

B.2 H diagram

The H diagram is most compactly expressed in terms of an extended notation

$$\dot{x}^M \equiv (\dot{x}_\mu; -i|\dot{x}|\Theta^I), \quad \partial_{x^M} \equiv (\partial_{x_\mu}; 0) \quad (67)$$

with $\mu = 0, \dots, 3$ and $I = 4, \dots, 9$, so that

$$\dot{x}^M = s\theta_0 (-s\tau, c\tau, 0, 0; i c\theta_0 c\tau, i c\theta_0 s\tau, -i s\theta_0, 0, 0, 0). \quad (68)$$

The contribution of this diagram is given by

$$H = \frac{\lambda^3}{8N^2} \left(\frac{1}{4\pi^2} \right)^5 \int d^4w \int d^4z \frac{H^M(w) H^M(z)}{(w-z)^2} \quad (69)$$

where

$$H^M(w) \equiv \int_0^{2\pi} d\tau \int_0^{2\pi} d\sigma \left[2\dot{y}^M (\dot{x} \cdot \partial_y) - 2\dot{x}^M (\dot{y} \cdot \partial_x) + [\dot{x} \cdot \dot{y} - \Theta_x \cdot \Theta_y |\dot{x}| |\dot{y}|] (\partial_{x^M} - \partial_{y^M}) \right] \times \frac{1}{(x-w)^2 (y-w)^2} \quad (70)$$

and $x = x(\tau) = (s\theta_0^1 c\tau, s\theta_0^1 s\tau, c\theta_0^1)$, $y = y(\sigma) = (s\theta_0^2 c\sigma, s\theta_0^2 s\sigma, c\theta_0^2)$, etc. One finds

$$\begin{aligned} H^4(w) &= -2i s\theta_0^1 s\theta_0^2 (c\theta_0^1 - c\theta_0^2) \left(I_s(\theta_0^2) (\partial_{w_0} I_c(\theta_0^1)) - I_c(\theta_0^2) (\partial_{w_0} I_s(\theta_0^1)) \right) \\ H^5(w) &= -2i s\theta_0^1 s\theta_0^2 (c\theta_0^1 - c\theta_0^2) \left(I_s(\theta_0^2) (\partial_{w_1} I_c(\theta_0^1)) - I_c(\theta_0^2) (\partial_{w_1} I_s(\theta_0^1)) \right) \\ H^6(w) &= 0 \end{aligned} \quad (71)$$

$$\begin{aligned} H^\mu(w) &= s\theta_0^1 s\theta_0^2 (1 - c\theta_0^1 c\theta_0^2) \left[I_c(\theta_0^1) (\partial_{w_\mu} I_c(\theta_0^2)) - I_c(\theta_0^2) (\partial_{w_\mu} I_c(\theta_0^1)) \right. \\ &\quad \left. + I_s(\theta_0^1) (\partial_{w_\mu} I_s(\theta_0^2)) - I_s(\theta_0^2) (\partial_{w_\mu} I_s(\theta_0^1)) \right] \\ &\quad - s^2 \theta_0^1 s^2 \theta_0^2 \left[I(\theta_0^1) (\partial_{w_\mu} I(\theta_0^2)) - I(\theta_0^2) (\partial_{w_\mu} I(\theta_0^1)) \right]. \end{aligned} \quad (72)$$

B.3 IY and two-rung bubble divergence cancellation

In this subsection we will demonstrate the cancellation of the divergence stemming from the two-rung bubble against the divergent part of the IY diagram. The finite parts left-over from this cancellation are calculated. The strategy follows [4] closely; Feynman parameters are introduced in favour of bulk integrations in order to demonstrate the cancellation, then the finite left-overs are re-cast in terms of bulk integrations.

The IY diagram is given by

$$\begin{aligned} IY &= \frac{\lambda^3}{8N^2} \int_0^{2\pi} d\vartheta \mathcal{F}(\vartheta) \oint d\tau_1 d\tau_2 d\sigma_1 E(\tau_1 \tau_2) \left\{ D(\tau_1, \sigma_1) [\dot{x}_2 \cdot \partial_{y_1} - \dot{x}_2 \cdot \partial_{x_1}] \right. \\ &\quad \left. + D(\tau_1, \tau_2) \dot{y}_1 \cdot \partial_{x_1} \right\} G(x_1, x_2, y_1) \end{aligned} \quad (73)$$

where

$$\mathcal{F}(\vartheta) = -\frac{(1 - c\theta_0^1 c\theta_0^2) \cos \vartheta + \Lambda}{8\pi^2 \cos \vartheta + \frac{1}{\Lambda}}, \quad \Lambda = \frac{s\theta_0^1 s\theta_0^2}{c\theta_0^1 c\theta_0^2 - 1}, \quad (74)$$

and

$$D(\tau, \sigma) = s\theta_0^1 s\theta_0^2 [(1 - c\theta_0^1 c\theta_0^2) \cos(\tau - \sigma) - s\theta_0^1 s\theta_0^2], \quad D(\tau_1, \tau_2) = s^4 \theta_0^1 (\cos \tau_{12} - 1), \quad (75)$$

and

$$E(\tau_1 \tau_2) \equiv 2\pi \operatorname{sgn}(\tau_1 - \tau_2) - 2(\tau_1 - \tau_2). \quad (76)$$

The triple-vertex kernel $G(x_1, x_2, y_1)$ is given in dimensional regularization ($d = 2\omega$) by

$$G(x_1, x_2, y_1) = \frac{\Gamma(2\omega - 3)}{2^6 \pi^{2\omega}} \int_0^1 d\alpha d\beta d\gamma \frac{(\alpha\beta\gamma)^{\omega-2} \delta(1 - \alpha - \beta - \gamma)}{[\alpha\beta(x_1 - x_2)^2 + \beta\gamma(x_2 - y_1)^2 + \alpha\gamma(x_1 - y_1)^2]^{2\omega-3}}. \quad (77)$$

We rewrite (73) as

$$IY = \frac{\lambda^3}{8N^2} \int_0^{2\pi} d\vartheta \mathcal{F}(\vartheta) \oint d\tau_1 d\tau_2 d\sigma_1 \frac{\Gamma(2\omega - 3)}{2^6 \pi^{2\omega}} \times 2(2\omega - 3) \int_0^1 d\alpha d\beta d\gamma (\alpha\beta\gamma)^{\omega-2} \delta(1 - \alpha - \beta - \gamma) \mathcal{O}, \quad (78)$$

where

$$\mathcal{O} \equiv \frac{E(\tau_1 \tau_2)}{\Delta^{2\omega-2}} \left\{ s\theta_0^1 s\theta_0^2 \left(\cos(\tau_1 - \sigma_1) [c\theta_0^1 c\theta_0^2 - 1] + s\theta_0^1 \theta_0^2 \right) \left((2\alpha + \beta)\gamma s\theta_0^1 s\theta_0^2 \sin(\sigma_1 - \tau_2) \right. \right. \\ \left. \left. - (2\gamma + \beta)\alpha s^2 \theta_0^1 \sin \tau_{12} \right) + s^4 \theta_0^1 (1 - \cos \tau_{12}) (2\beta + \gamma)\alpha s\theta_0^1 s\theta_0^2 \sin(\tau_1 - \sigma_1) \right\}, \quad (79)$$

and where

$$\Delta = 2\alpha\beta s^2 \theta_0^1 (1 - \cos \tau_{12}) + 2\beta\gamma \left(1 - s\theta_0^1 s\theta_0^2 \cos(\tau_2 - \sigma_1) - c\theta_0^1 c\theta_0^2 \right) \\ + 2\alpha\gamma \left(1 - s\theta_0^1 s\theta_0^2 \cos(\tau_1 - \sigma_1) - c\theta_0^1 c\theta_0^2 \right). \quad (80)$$

After [4] we consider the following total derivatives

$$\begin{aligned}
K_1 = & -\frac{1}{2} (\cos \theta_0^1 \cos \theta_0^2 - 1) \sin^2 \theta_0^1 \partial_{\tau_2} \left(E(\tau_1 \tau_2) \frac{(1 - \cos \tau_{12})}{\Delta^{2\omega-3}} \right) = \\
& -\frac{s^2 \theta_0^1}{2} (c\theta_0^1 c\theta_0^2 - 1) [-4\pi\delta(\tau_{12}) + 2] \frac{(1 - \cos \tau_{12})}{\Delta^{2\omega-3}} \\
& + \frac{s^2 \theta_0^1}{2} (c\theta_0^1 c\theta_0^2 - 1) E(\tau_1 \tau_2) \frac{\sin \tau_{12}}{\Delta^{2\omega-3}} \\
& - s^2 \theta_0^1 (c\theta_0^1 c\theta_0^2 - 1) E(\tau_1 \tau_2) (3 - 2\omega)(1 - \cos \tau_{12}) \\
& \quad \times \frac{-\alpha\beta s^2 \theta_0^1 \sin \tau_{12} - \beta\gamma s \theta_0^1 s \theta_0^2 \sin(\sigma_1 - \tau_2)}{\Delta^{2\omega-2}}
\end{aligned} \tag{81}$$

$$\begin{aligned}
K_2 = & s\theta_0^1 s\theta_0^2 \partial_{\tau_1} \left(E(\tau_1 \tau_2) \frac{\cos(\tau_1 - \sigma_1)[c\theta_0^1 c\theta_0^2 - 1] + s\theta_0^1 s\theta_0^2}{\Delta^{2\omega-3}} \right) = \\
& s\theta_0^1 s\theta_0^2 [4\pi\delta(\tau_{12}) - 2] \frac{\cos(\tau_1 - \sigma_1)[c\theta_0^1 c\theta_0^2 - 1] + s\theta_0^1 s\theta_0^2}{\Delta^{2\omega-3}} \\
& - s\theta_0^1 s\theta_0^2 E(\tau_1 \tau_2) [c\theta_0^1 c\theta_0^2 - 1] \frac{\sin(\tau_1 - \sigma_1)}{\Delta^{2\omega-3}} \\
& + s\theta_0^1 s\theta_0^2 2(3 - 2\omega) E(\tau_1 \tau_2) (\cos(\tau_1 - \sigma_1)[c\theta_0^1 c\theta_0^2 - 1] + s\theta_0^1 s\theta_0^2) \\
& \quad \times \frac{[\alpha\beta s^2 \theta_0^1 \sin \tau_{12} - \alpha\gamma s \theta_0^1 s \theta_0^2 \sin(\sigma_1 - \tau_1)]}{\Delta^{2\omega-2}}
\end{aligned} \tag{82}$$

$$\begin{aligned}
K_3 = & \frac{s\theta_0^1 s\theta_0^2}{2} \partial_{\tau_2} \left(E(\tau_1 \tau_2) \frac{\cos(\tau_1 - \sigma_1)[c\theta_0^1 c\theta_0^2 - 1] + s\theta_0^1 s\theta_0^2}{\Delta^{2\omega-3}} \right) = \\
& \frac{s\theta_0^1 s\theta_0^2}{2} [-4\pi\delta(\tau_{12}) + 2] \frac{\cos(\tau_1 - \sigma_1)[c\theta_0^1 c\theta_0^2 - 1] + s\theta_0^1 s\theta_0^2}{\Delta^{2\omega-3}} \\
& + s\theta_0^1 s\theta_0^2 (3 - 2\omega) E(\tau_1 \tau_2) (\cos(\tau_1 - \sigma_1)[c\theta_0^1 c\theta_0^2 - 1] + s\theta_0^1 s\theta_0^2) \\
& \quad \times \frac{[-\alpha\beta s^2 \theta_0^1 \sin \tau_{12} - \beta\gamma s \theta_0^1 s \theta_0^2 \sin(\sigma_1 - \tau_2)]}{\Delta^{2\omega-2}}
\end{aligned} \tag{83}$$

The sum of the three RHS's may be expressed as follows (where we use manipulations valid under the integrations in (78))

$K_1 + K_2 + K_3 =$

$$\begin{aligned}
& 2\pi\delta(\tau_{12}) s\theta_0^1 s\theta_0^2 \frac{\cos(\tau_1 - \sigma_1)[c\theta_0^1 c\theta_0^2 - 1] + s\theta_0^1 s\theta_0^2}{\Delta^{2\omega-3}} \\
& - s^2\theta_0^1 (c\theta_0^1 c\theta_0^2 - 1) \frac{(1 - \cos \tau_{12})}{\Delta^{2\omega-3}} - s\theta_0^1 s\theta_0^2 \frac{\cos(\tau_1 - \sigma_1)[c\theta_0^1 c\theta_0^2 - 1] + s\theta_0^1 s\theta_0^2}{\Delta^{2\omega-3}} \\
& + \frac{s^2\theta_0^1}{2} (c\theta_0^1 c\theta_0^2 - 1) E(\tau_1 \tau_2) \frac{\sin \tau_{12}}{\Delta^{2\omega-3}} + s\theta_0^1 s\theta_0^2 E(\tau_1 \tau_2) (1 - c\theta_0^1 c\theta_0^2) \frac{\sin(\tau_1 - \sigma_1)}{\Delta^{2\omega-3}} \\
& + (3 - 2\omega) s^2\theta_0^1 (c\theta_0^1 c\theta_0^2 - 1) E(\tau_1 \tau_2) (1 - \cos \tau_{12}) \frac{s^2\theta_0^1 \alpha \beta \sin \tau_{12} + s\theta_0^1 s\theta_0^2 \beta \gamma \sin(\sigma_1 - \tau_2)}{\Delta^{2\omega-2}} \\
& + (3 - 2\omega) s\theta_0^1 s\theta_0^2 E(\tau_1 \tau_2) (\cos(\tau_1 - \sigma_1)[c\theta_0^1 c\theta_0^2 - 1] + s\theta_0^1 s\theta_0^2) \\
& \times \frac{s^2\theta_0^1 \alpha \beta \sin \tau_{12} - 2s\theta_0^1 s\theta_0^2 \alpha \gamma \sin(\sigma_1 - \tau_1) - s\theta_0^1 s\theta_0^2 \beta \gamma \sin(\sigma_1 - \tau_2)}{\Delta^{2\omega-2}}.
\end{aligned} \tag{84}$$

We would now like to reconstitute (79) using the terms proportional to $E(\tau_1 \tau_2)$ in (84). We do this by first stripping-off terms proportional to $(4 - 2\omega)$ by writing $(3 - 2\omega) = (4 - 2\omega) - 1$. We define

$$\begin{aligned}
\Psi \equiv \frac{E(\tau_1 \tau_2)}{\Delta^{2\omega-2}} & \left\{ \frac{s^2\theta_0^1}{2} (c\theta_0^1 c\theta_0^2 - 1) \sin \tau_{12} \Delta + s\theta_0^1 s\theta_0^2 (1 - c\theta_0^1 c\theta_0^2) \sin(\tau_1 - \sigma_1) \Delta \right. \\
& - s^2\theta_0^1 (c\theta_0^1 c\theta_0^2 - 1) (1 - \cos \tau_{12}) \left(s^2\theta_0^1 \alpha \beta \sin \tau_{12} + s\theta_0^1 s\theta_0^2 \beta \gamma \sin(\sigma_1 - \tau_2) \right) \\
& - s\theta_0^1 s\theta_0^2 (\cos(\tau_1 - \sigma_1)[c\theta_0^1 c\theta_0^2 - 1] + s\theta_0^1 s\theta_0^2) \\
& \left. \times \left(s^2\theta_0^1 \alpha \beta \sin \tau_{12} - 2s\theta_0^1 s\theta_0^2 \alpha \gamma \sin(\sigma_1 - \tau_1) - s\theta_0^1 s\theta_0^2 \beta \gamma \sin(\sigma_1 - \tau_2) \right) \right\},
\end{aligned} \tag{85}$$

so that

$$\begin{aligned}
\sum_i K_i &= \Psi + 2\pi\delta(\tau_{12}) s\theta_0^1 s\theta_0^2 \frac{\cos(\tau_1 - \sigma_1)[c\theta_0^1 c\theta_0^2 - 1] + s\theta_0^1 s\theta_0^2}{\Delta^{2\omega-3}} \\
& - s^2\theta_0^1 (c\theta_0^1 c\theta_0^2 - 1) \frac{(1 - \cos \tau_{12})}{\Delta^{2\omega-3}} - s\theta_0^1 s\theta_0^2 \frac{\cos(\tau_1 - \sigma_1)[c\theta_0^1 c\theta_0^2 - 1] + s\theta_0^1 s\theta_0^2}{\Delta^{2\omega-3}} \\
& + (4 - 2\omega) s^2\theta_0^1 (c\theta_0^1 c\theta_0^2 - 1) E(\tau_1 \tau_2) (1 - \cos \tau_{12}) \frac{s^2\theta_0^1 \alpha \beta \sin \tau_{12} + s\theta_0^1 s\theta_0^2 \beta \gamma \sin(\sigma_1 - \tau_2)}{\Delta^{2\omega-2}} \\
& + (4 - 2\omega) s\theta_0^1 s\theta_0^2 E(\tau_1 \tau_2) (\cos(\tau_1 - \sigma_1)[c\theta_0^1 c\theta_0^2 - 1] + s\theta_0^1 s\theta_0^2) \\
& \times \frac{s^2\theta_0^1 \alpha \beta \sin \tau_{12} - 2s\theta_0^1 s\theta_0^2 \alpha \gamma \sin(\sigma_1 - \tau_1) - s\theta_0^1 s\theta_0^2 \beta \gamma \sin(\sigma_1 - \tau_2)}{\Delta^{2\omega-2}},
\end{aligned} \tag{86}$$

then, expressing the last two terms with derivatives, we have

$$\begin{aligned}
&= \Psi + 2\pi\delta(\tau_{12}) s\theta_0^1 s\theta_0^2 \frac{\cos(\tau_1 - \sigma_1)[c\theta_0^1 c\theta_0^2 - 1] + s\theta_0^1 s\theta_0^2}{\Delta^{2\omega-3}} \\
&\quad - s^2\theta_0^1 (c\theta_0^1 c\theta_0^2 - 1) \frac{(1 - \cos \tau_{12})}{\Delta^{2\omega-3}} - s\theta_0^1 s\theta_0^2 \frac{\cos(\tau_1 - \sigma_1)[c\theta_0^1 c\theta_0^2 - 1] + s\theta_0^1 s\theta_0^2}{\Delta^{2\omega-3}} \\
&\quad + \frac{(4-2\omega)}{(3-2\omega)} \frac{s^2\theta_0^1}{2} (c\theta_0^1 c\theta_0^2 - 1) E(\tau_1 \tau_2) (1 - \cos \tau_{12}) (-\partial_{\tau_2}) \frac{1}{\Delta^{2\omega-3}} \\
&\quad + \frac{(4-2\omega)}{(3-2\omega)} s\theta_0^1 s\theta_0^2 E(\tau_1 \tau_2) (\cos(\tau_1 - \sigma_1)[c\theta_0^1 c\theta_0^2 - 1] + s\theta_0^1 s\theta_0^2) \left(\partial_{\tau_1} + \frac{1}{2}\partial_{\tau_2} \right) \frac{1}{\Delta^{2\omega-3}}, \tag{87}
\end{aligned}$$

then using integration by parts in τ_1, τ_2 ,

$$\begin{aligned}
&= \Psi - \frac{2\pi\delta(\tau_{12})}{(3-2\omega)} s\theta_0^1 s\theta_0^2 \frac{\cos(\tau_1 - \sigma_1)[c\theta_0^1 c\theta_0^2 - 1] + s\theta_0^1 s\theta_0^2}{\Delta^{2\omega-3}} \\
&\quad + \frac{s^2\theta_0^1 (c\theta_0^1 c\theta_0^2 - 1)}{(3-2\omega)} \frac{(1 - \cos \tau_{12})}{\Delta^{2\omega-3}} + \frac{s\theta_0^1 s\theta_0^2 \cos(\tau_1 - \sigma_1)[c\theta_0^1 c\theta_0^2 - 1] + s\theta_0^1 s\theta_0^2}{(3-2\omega) \Delta^{2\omega-3}} \\
&\quad - \frac{(4-2\omega)}{(3-2\omega)} \frac{E(\tau_1 \tau_2)}{\Delta^{2\omega-3}} (c\theta_0^1 c\theta_0^2 - 1) \left(\frac{s^2\theta_0^1}{2} \sin \tau_{12} - s\theta_0^1 s\theta_0^2 \sin(\tau_1 - \sigma_1) \right). \tag{88}
\end{aligned}$$

One can then show that

$$\begin{aligned}
\mathcal{O} &= \Psi + \frac{E(\tau_1 \tau_2)}{\Delta^{2\omega-2}} (c\theta_0^1 - c\theta_0^2)^2 \gamma(1 - \gamma) \left(s^2\theta_0^1 \sin \tau_{12} - 2s\theta_0^1 s\theta_0^2 \sin(\tau_1 - \sigma_1) \right) \\
&\quad + \frac{E(\tau_1 \tau_2)}{\Delta^{2\omega-2}} s^3\theta_0^1 s\theta_0^2 c\theta_0^1 (c\theta_0^2 - c\theta_0^1) (2\beta + \gamma) \alpha (1 - \cos \tau_{12}) \sin(\tau_1 - \sigma_1), \tag{89}
\end{aligned}$$

and therefore

$$\mathcal{O} = \text{total deriv.} + (IY)_{SE} + (IY)_1 + (IY)_2 + (IY)_3 + (IY)_{\omega-2}, \tag{90}$$

since $\sum K_i$ is a total derivative, and where we have introduced

$$\begin{aligned}
(IY)_{SE} &= \frac{2\pi\delta(\tau_{12})}{(3-2\omega)} s\theta_0^1 s\theta_0^2 \frac{\cos(\tau_1 - \sigma_1)[c\theta_0^1 c\theta_0^2 - 1] + s\theta_0^1 s\theta_0^2}{\Delta^{2\omega-3}} \\
(IY)_1 &= -\frac{s^2\theta_0^1 (c\theta_0^1 c\theta_0^2 - 1)}{(3-2\omega)} \frac{(1 - \cos \tau_{12})}{\Delta^{2\omega-3}} - \frac{s\theta_0^1 s\theta_0^2 \cos(\tau_1 - \sigma_1)[c\theta_0^1 c\theta_0^2 - 1] + s\theta_0^1 s\theta_0^2}{(3-2\omega) \Delta^{2\omega-3}} \tag{91}
\end{aligned}$$

$$\begin{aligned}
(IY)_2 &= \frac{E(\tau_1 \tau_2)}{\Delta^{2\omega-2}} (c\theta_0^1 - c\theta_0^2)^2 \gamma(1 - \gamma) \left(s^2\theta_0^1 \sin \tau_{12} - 2s\theta_0^1 s\theta_0^2 \sin(\tau_1 - \sigma_1) \right) \\
(IY)_3 &= \frac{E(\tau_1 \tau_2)}{\Delta^{2\omega-2}} s^3\theta_0^1 s\theta_0^2 c\theta_0^1 (c\theta_0^2 - c\theta_0^1) (2\beta + \gamma) \alpha (1 - \cos \tau_{12}) \sin(\tau_1 - \sigma_1) \tag{92} \\
(IY)_{\omega-2} &= \frac{(4-2\omega)}{(3-2\omega)} \frac{E(\tau_1 \tau_2)}{\Delta^{2\omega-3}} (c\theta_0^1 c\theta_0^2 - 1) \left(\frac{s^2\theta_0^1}{2} \sin \tau_{12} - s\theta_0^1 s\theta_0^2 \sin(\tau_1 - \sigma_1) \right).
\end{aligned}$$

Plugging these forms back into (78) one finds that half of the 1-loop corrected two-rung diagram is canceled by $(IY)_{SE}$ (the $\theta_0^1 \leftrightarrow \theta_0^2$ piece takes care of the other half), and that $(IY)_{\omega=2}$ is zero on the physical dimension $\omega = 2$. The remaining terms $(IY)_{1,2,3}$ are finite on the physical dimension and must be evaluated (along with their $\theta_0^1 \leftrightarrow \theta_0^2$ counterparts). In the following subsections we recast $(IY)_{1,2,3}$ in terms of bulk integrations.

B.3.1 $(IY)_1$

Plugging $(IY)_1$ from (91) into (78), and reverting to bulk integration, one finds

$$\begin{aligned} \Pi_1 = & \frac{\lambda^3}{4N^2} \frac{1}{4\pi} (c\theta_0^1 c\theta_0^2 - 1 + |c\theta_0^1 - c\theta_0^2|) \frac{1}{64\pi^6} \oint d\tau_1 d\tau_2 d\sigma_1 \\ & \times \int d^4w \frac{s^2\theta_0^1 (c\theta_0^1 c\theta_0^2 - 1) (1 - \cos \tau_{12}) + s\theta_0^1 s\theta_0^2 (\cos(\tau_1 - \sigma_1) [c\theta_0^1 c\theta_0^2 - 1] + s\theta_0^1 s\theta_0^2)}{(x_1 - w)^2 (x_2 - w)^2 (y_1 - w)^2}, \end{aligned} \quad (93)$$

where we have used the result

$$\int_0^{2\pi} d\vartheta \mathcal{F}(\vartheta) = \frac{1}{4\pi} (c\theta_0^1 c\theta_0^2 - 1 + |c\theta_0^1 - c\theta_0^2|). \quad (94)$$

We now continue by integrating over τ_1, τ_2 , and σ_1 . We find

$$\begin{aligned} \Pi_1 = & \frac{\lambda^3}{4N^2} \frac{1}{4\pi} (c\theta_0^1 c\theta_0^2 - 1 + |c\theta_0^1 - c\theta_0^2|) \frac{1}{64\pi^6} \int d^4w \\ & \times \left[s^2\theta_0^1 c\theta_0^2 (c\theta_0^1 - c\theta_0^2) I^2(\theta_0^1) I(\theta_0^2) - s^2\theta_0^1 (c\theta_0^1 c\theta_0^2 - 1) (I_c^2(\theta_0^1) + I_s^2(\theta_0^1)) I(\theta_0^2) \right. \\ & \left. + s\theta_0^1 s\theta_0^2 (c\theta_0^1 c\theta_0^2 - 1) (I_c(\theta_0^1) I_c(\theta_0^2) + I_s(\theta_0^1) I_s(\theta_0^2)) I(\theta_0^1) \right]. \end{aligned} \quad (95)$$

B.3.2 $(IY)_2$

This contribution is significantly more complicated due to the presence of the $E(\tau_1 \tau_2)$ in the integrand. Plugging $(IY)_2$ from (92) into (78), we need to evaluate

$$\begin{aligned} \Pi_2 = & \frac{\lambda^3}{4N^2} \frac{1}{4\pi} (c\theta_0^1 c\theta_0^2 - 1 + |c\theta_0^1 - c\theta_0^2|) (c\theta_0^1 - c\theta_0^2)^2 \frac{1}{2(c\theta_0^1 - c\theta_0^2)} \frac{\partial}{\partial(c\theta_0^2)} \frac{1}{64\pi^6} \int d^4w \\ & \times \oint d\tau_1 d\tau_2 d\sigma_1 E(\tau_1 \tau_2) \frac{(s^2\theta_0^1 \sin \tau_{12} - 2s\theta_0^1 s\theta_0^2 \sin(\tau_1 - \sigma_1))}{(x_1 - w)^2 (x_2 - w)^2 (y_1 - w)^2}, \end{aligned} \quad (96)$$

where we treat $c\theta_0^2$ and $s\theta_0^2$ as independent variables for the purposes of differentiation, and therefore must be cautious not to use trigonometric identities which relate them until after the derivative has been taken. With this prescription

$$\begin{aligned} \Delta = & 2\alpha\beta s^2\theta_0^1(1 - \cos \tau_{12}) + \beta\gamma [s^2\theta_0^1 + s^2\theta_0^2 + (c\theta_0^1 - c\theta_0^2)^2 - 2s\theta_0^1s\theta_0^2 \cos(\tau_2 - \sigma_1)] \\ & + \alpha\gamma [s^2\theta_0^1 + s^2\theta_0^2 + (c\theta_0^1 - c\theta_0^2)^2 - 2s\theta_0^1s\theta_0^2 \cos(\tau_1 - \sigma_1)], \end{aligned} \quad (97)$$

and hence the factor $\gamma(1 - \gamma)$ in (92) is obtained through the derivative in $c\theta_0$. The evaluation of the integrals over τ_1, τ_2 , and σ_1 are as in [4]. The results are

$$\begin{aligned} \mathcal{C}_1 \equiv & \oint d\tau_1 d\tau_2 d\sigma_1 E(\tau_1 \tau_2) \frac{\sin \tau_{12}}{(x_1 - w)^2 (x_2 - w)^2 (y_1 - w)^2} \\ = & \frac{64\pi^3}{\sqrt{a_1^2 - (b_1^2 + c_1^2)}\sqrt{a_2^2 - (b_2^2 + c_2^2)}} \frac{a_1}{(b_1^2 + c_1^2)} \ln \left(\frac{a_1 + \sqrt{a_1^2 - (b_1^2 + c_1^2)}}{2\sqrt{a_1^2 - (b_1^2 + c_1^2)}} \right) \end{aligned} \quad (98)$$

$$\begin{aligned} \mathcal{C}_2 \equiv & \oint d\tau_1 d\tau_2 d\sigma_1 E(\tau_1 \tau_2) \frac{\sin(\tau_1 - \sigma_1)}{(x_1 - w)^2 (x_2 - w)^2 (y_1 - w)^2} \\ = & \frac{32\pi^3}{\sqrt{a_1^2 - (b_1^2 + c_1^2)}\sqrt{a_2^2 - (b_2^2 + c_2^2)}} \frac{b_1b_2 + c_1c_2}{(b_1^2 + c_1^2) [a_2 + \sqrt{a_2^2 - (b_2^2 + c_2^2)}]} \\ & \times \ln \left(\frac{a_1 + \sqrt{a_1^2 - (b_1^2 + c_1^2)}}{2\sqrt{a_1^2 - (b_1^2 + c_1^2)}} \right) \end{aligned} \quad (99)$$

where the $\{a, b, c\}_i$ are given by (63) and where the index refers to either θ_0^1 or θ_0^2 . We therefore have that

$$\Pi_2 = \frac{\lambda^3}{4N^2} \frac{1}{4\pi} (c\theta_0^1c\theta_0^2 - 1 + |c\theta_0^1 - c\theta_0^2|) \frac{(c\theta_0^1 - c\theta_0^2)}{2} \frac{1}{64\pi^6} \int d^4w \partial_{c\theta_0^2} (s^2\theta_0^1 \mathcal{C}_1 - 2s\theta_0^1s\theta_0^2 \mathcal{C}_2). \quad (100)$$

B.3.3 $(IY)_3$

Looking at (92) we see that we must express the integrand

$$\frac{E(\tau_1 \tau_2)}{\Delta^{2\omega-2}} (2\alpha\beta + \alpha\gamma)(1 - \cos \tau_{12}) \sin(\tau_1 - \sigma_1) \quad (101)$$

without Feynman parameters. Referring to (97), and again treating $s\theta_0$ and $c\theta_0$ as independent, we see that

$$\begin{aligned}
\partial_{s\theta_0^1}\Delta &= 4\alpha\beta s\theta_0^1(1 - \cos \tau_{12}) + 2\beta\gamma(s\theta_0^1 - s\theta_0^2 \cos(\tau_2 - \sigma_1)) + 2\alpha\gamma(s\theta_0^1 - s\theta_0^2 \cos(\tau_1 - \sigma_1)) \\
\partial_{s\theta_0^2}\Delta &= 2\beta\gamma(s\theta_0^2 - s\theta_0^1 \cos(\tau_2 - \sigma_1)) + 2\alpha\gamma(s\theta_0^2 - s\theta_0^1 \cos(\tau_1 - \sigma_1))
\end{aligned} \tag{102}$$

and therefore

$$\left(s\theta_0^1\partial_{s\theta_0^1} - s\theta_0^2\partial_{s\theta_0^2}\right)\Delta = 4\alpha\beta s^2\theta_0^1(1 - \cos \tau_{12}) + 2\gamma(1 - \gamma)(s^2\theta_0^1 - s^2\theta_0^2). \tag{103}$$

Whereas

$$\begin{aligned}
(1 - \cos \tau_{12})\partial_{\tau_1}\Delta &= (1 - \cos \tau_{12}) \left[2\alpha\beta s^2\theta_0^1 \sin \tau_{12} + 2\alpha\gamma s\theta_0^1 s\theta_0^2 \sin(\tau_1 - \sigma_1)\right] \\
&= \sin \tau_{12} \left[\Delta - \beta\gamma \left[s^2\theta_0^1 + s^2\theta_0^2 + (c\theta_0^1 - c\theta_0^2)^2 - 2s\theta_0^1 s\theta_0^2 \cos(\tau_2 - \sigma_1)\right] \right. \\
&\quad \left. - \alpha\gamma \left[s^2\theta_0^1 + s^2\theta_0^2 + (c\theta_0^1 - c\theta_0^2)^2 - 2s\theta_0^1 s\theta_0^2 \cos(\tau_1 - \sigma_1)\right] \right] \\
&\quad + 2\alpha\gamma s\theta_0^1 s\theta_0^2 \sin(\tau_1 - \sigma_1)(1 - \cos \tau_{12}) \\
&= \sin \tau_{12} \left[\Delta - \gamma(1 - \gamma) \left[s^2\theta_0^1 - s^2\theta_0^2 + (c\theta_0^1 - c\theta_0^2)^2\right] - s\theta_0^2 \partial_{s\theta_0^2}\Delta \right] \\
&\quad + 2\alpha\gamma s\theta_0^1 s\theta_0^2 \sin(\tau_1 - \sigma_1)(1 - \cos \tau_{12}).
\end{aligned} \tag{104}$$

We therefore have that

$$\begin{aligned}
\frac{(2\alpha\beta + \alpha\gamma)(1 - \cos \tau_{12}) \sin(\tau_1 - \sigma_1)}{\Delta^{2\omega-2}} &= \frac{\left(s\theta_0^1\partial_{s\theta_0^1} - s\theta_0^2\partial_{s\theta_0^2}\right) \sin(\tau_1 - \sigma_1)}{2(3 - 2\omega)s^2\theta_0^1 \Delta^{2\omega-3}} \\
&\quad - \gamma(1 - \gamma) \frac{(s^2\theta_0^1 - s^2\theta_0^2) \sin(\tau_1 - \sigma_1)}{s^2\theta_0^1 \Delta^{2\omega-2}} + \frac{(1 - \cos \tau_{12})}{2(3 - 2\omega)s\theta_0^1 s\theta_0^2} \partial_{\tau_1} \frac{1}{\Delta^{2\omega-3}} \\
&\quad - \frac{\sin \tau_{12}}{2s\theta_0^1 s\theta_0^2} \frac{1}{\Delta^{2\omega-3}} + \frac{\sin \tau_{12}}{2(3 - 2\omega)s\theta_0^1} \partial_{s\theta_0^2} \frac{1}{\Delta^{2\omega-3}} \\
&\quad + \gamma(1 - \gamma) \sin \tau_{12} \frac{[s^2\theta_0^1 - s^2\theta_0^2 + (c\theta_0^1 - c\theta_0^2)^2]}{2s\theta_0^1 s\theta_0^2} \frac{1}{\Delta^{2\omega-2}}.
\end{aligned} \tag{105}$$

We now can express the $\gamma(1 - \gamma)$ as a derivative in $c\theta_0^2$, as per the previous subsection. Further we note that under integration (and for $\omega = 2$)

$$E(\tau_1 \tau_2) \left[\frac{(1 - \cos \tau_{12})}{2(3 - 2\omega)s\theta_0^1 s\theta_0^2} \partial_{\tau_1} \frac{1}{\Delta^{2\omega-3}} - \frac{\sin \tau_{12}}{2s\theta_0^1 s\theta_0^2} \frac{1}{\Delta^{2\omega-3}} \right] = \frac{(1 - \cos \tau_{12})}{(3 - 2\omega)s\theta_0^1 s\theta_0^2} \frac{1}{\Delta^{2\omega-3}} \tag{106}$$

by integration by parts in τ_1 . The RHS is then integrated as per $(IY)_1$, and expressed in terms of $I(\theta_0)$, $I_c(\theta_0)$, $I_s(\theta_0)$. The $(IY)_3$ contribution from (92), once plugged-in to (78), is then expressed as

$$\begin{aligned}
\Pi_3 = & \frac{\lambda^3}{4N^2} \frac{1}{4\pi} (c\theta_0^1 c\theta_0^2 - 1 + |c\theta_0^1 - c\theta_0^2|) s^3 \theta_0^1 s\theta_0^2 c\theta_0^1 (c\theta_0^1 - c\theta_0^2) \frac{1}{64\pi^6} \int d^4w \\
& \times \left\{ \frac{1}{2s\theta_0^1 s\theta_0^2} \left(s\theta_0^2 \partial_{s\theta_0^2} + c\theta_0^2 \partial_{c\theta_0^2} \right) \mathcal{C}_1 \right. \\
& + \frac{1}{2s^2\theta_0^1} \left(s\theta_0^1 \partial_{s\theta_0^1} - s\theta_0^2 \partial_{s\theta_0^2} - (c\theta_0^1 + c\theta_0^2) \partial_{c\theta_0^2} \right) \mathcal{C}_2 \\
& \left. + \frac{1}{s\theta_0^1 s\theta_0^2} I(\theta_0^2) [I^2(\theta_0^1) - I_c^2(\theta_0^1) - I_s^2(\theta_0^1)] \right\}. \tag{107}
\end{aligned}$$

B.4 The coincident limit

In what follows we will make extensive use of the integrals collected in (62). To simplify things we cast them in a simpler form

$$\begin{aligned}
I(\theta_0) = \frac{2\pi}{\sqrt{L^+L^-}}, \quad I_c(\theta_0) = \frac{4\pi s\theta_0 w_0}{\sqrt{L^+L^-(a + \sqrt{L^+L^-})}}, \quad I_s(\theta_0) = \frac{4\pi s\theta_0 w_1}{\sqrt{L^+L^-(a + \sqrt{L^+L^-})}}, \\
\text{where } L^\pm \equiv (\rho \pm s\theta_0)^2 + (w_2 - c\theta_0)^2 + w_3^2, \quad a \equiv \rho^2 + s^2\theta_0 + (w_2 - c\theta_0)^2 + w_3^2. \tag{108}
\end{aligned}$$

The L^\pm and a are found also in the \mathcal{C}_i integrals defined in (98) and (99). In order to extract the leading behaviour as $\theta_0^1 \rightarrow \theta_0^2$ we can borrow from the analysis carried out in [4] for the case of 1/2 BPS circles in the coincident limit. The observation is that the integration over the bulk space-time interaction point w is dominated in this limit by the region $\rho = \sqrt{w_0^2 + w_1^2} \simeq s\theta_0^1 \simeq s\theta_0^2$, $w_2 \simeq c\theta_0^1 \simeq c\theta_0^2$, and $w_3 \simeq 0$. This is the region where $L^- \simeq 0$, $L^+ \simeq 4s^2\theta_0$, and $a \simeq 2s^2\theta_0$. In the special case of the H diagram where there are two space-time interaction points, both integrations are dominated by this same region. The $\theta_0^1 \rightarrow \theta_0^2$ limit is then taken as follows:

1. Combine integrands with their $\theta_0^1 \leftrightarrow \theta_0^2$ counterparts.
2. In the denominator, replace L^+ by $4s^2\theta_0$, a by $2s^2\theta_0$, and $a + \sqrt{L^+L^-}$ by $2s^2\theta_0$.
3. Shift $\rho \rightarrow \rho + s\theta_0^1$, $w_2 \rightarrow w_2 + c\theta_0^1$.
4. Scale all components of w by $|h|$, where $h \equiv c\theta_0^1 - c\theta_0^2$.
5. If resulting integral is divergent as $w \rightarrow \infty$, it should be cut-off at $\mathcal{O}(1/h)$.

B.4.1 X diagram

The leading result for the X-diagram goes as $|h|$, specifically one finds from (66)

$$\begin{aligned}
X & \simeq \frac{\lambda^3}{8N^2} \left(\frac{1}{4\pi^2} \right)^4 8\pi^8 s^4 \theta_0 |c\theta_0^1 - c\theta_0^2| \\
& = \frac{\lambda^3}{8N^2} \frac{1}{32} s^4 \theta_0 |h|. \tag{109}
\end{aligned}$$

B.4.2 H diagram

Taking the coincident limit, we find that the leading terms are of order $|h|^0$ and come from H^μ , i.e. (72). These are then cancelled by their $\theta_0^1 \leftrightarrow \theta_0^2$ counterparts. We give an example of such a term below, which stems from the first two components of H^μ

$$\frac{\lambda^3 s^5 \theta_0}{N^2 2^{12} \pi^4} |h| \int_{-\infty}^{\infty} d\rho d\bar{\rho} dw_2 dw_3 dz_2 dz_3 \frac{\rho + \cot \theta_0}{\sqrt{R_1(w)R_2(w)}} \frac{1}{\sqrt{(\rho - \bar{\rho})^2 + (w_2 - z_2)^2 + (w_3 - z_3)^2}} \frac{\bar{\rho} + \cot \theta_0}{\sqrt{R_1(z)R_2(z)}} = \mathcal{O}(h^0) \quad (110)$$

where the R_i are defined in (64). The integral is linearly divergent and therefore supplies a factor of $1/|h|$. The $\theta_0^1 \leftrightarrow \theta_0^2$ counterpart cancels this contribution. We find that all such contributions from H^μ behave as above, and we therefore have that

$$H < \mathcal{O}(h^0). \quad (111)$$

B.4.3 IY diagram

In taking the coincident limit one finds that the leading contributions go as $|h| \log |h|$ and come from $(IY)_3$, i.e. (107). One finds the contribution

$$-\frac{\lambda^3 s^2 \theta_0 c \theta_0}{N^2 256 \pi^3} |h| \log |h| \int_{-\infty}^{\infty} d\rho dw_2 dw_3 \times \frac{2\rho(\rho^2 + w_2^2 + w_3^2) + \cot \theta_0(3\rho^2 + w_2^2 + w_3^2) - 2w_2\rho + \rho(1 + \cot^2 \theta_0)}{R_1(w)^{3/2} R_2(w)^{3/2}} = 0 \quad (112)$$

where the R_i are defined in (64). The integral happens to evaluate to zero, and is in any case cancelled by the $\theta_0^1 \leftrightarrow \theta_0^2$ counterpart. Therefore we have that

$$(IY)_1 + (IY)_2 + (IY)_3 < \mathcal{O}(|h| \log |h|). \quad (113)$$

References

- [1] J. M. Maldacena, “Wilson loops in large N field theories,” *Phys. Rev. Lett.* **80**, 4859 (1998) [arXiv:hep-th/9803002].
- [2] N. Drukker, D. J. Gross and H. Ooguri, “Wilson loops and minimal surfaces,” *Phys. Rev. D* **60**, 125006 (1999) [arXiv:hep-th/9904191].
- [3] J. M. Maldacena, “The large N limit of superconformal field theories and supergravity,” *Adv. Theor. Math. Phys.* **2**, 231 (1998) [*Int. J. Theor. Phys.* **38**, 1113 (1999)] [arXiv:hep-th/9711200].
- [4] J. Plefka and M. Staudacher, “Two loops to two loops in N = 4 supersymmetric Yang-Mills theory,” *JHEP* **0109**, 031 (2001) [arXiv:hep-th/0108182].

- [5] G. Arutyunov, J. Plefka and M. Staudacher, “Limiting geometries of two circular Maldacena-Wilson loop operators,” JHEP **0112**, 014 (2001) [arXiv:hep-th/0111290].
- [6] K. Zarembo, “Supersymmetric Wilson loops,” Nucl. Phys. B **643**, 157 (2002) [arXiv:hep-th/0205160].
- [7] Z. Guralnik and B. Kulik, “Properties of chiral Wilson loops,” JHEP **0401**, 065 (2004) [arXiv:hep-th/0309118].
- [8] A. Dymarsky, S. S. Gubser, Z. Guralnik and J. M. Maldacena, “Calibrated surfaces and supersymmetric Wilson loops,” JHEP **0609**, 057 (2006) [arXiv:hep-th/0604058].
- [9] J. K. Erickson, G. W. Semenoff and K. Zarembo, “Wilson loops in $N = 4$ supersymmetric Yang-Mills theory,” Nucl. Phys. B **582**, 155 (2000) [arXiv:hep-th/0003055].
- [10] N. Drukker and D. J. Gross, “An exact prediction of $N = 4$ SUSYM theory for string theory,” J. Math. Phys. **42**, 2896 (2001) [arXiv:hep-th/0010274].
- [11] N. Drukker and B. Fiol, “All-genus calculation of Wilson loops using D-branes,” JHEP **0502**, 010 (2005) [arXiv:hep-th/0501109].
- [12] J. Gomis and F. Passerini, “Holographic Wilson loops,” JHEP **0608**, 074 (2006) [arXiv:hep-th/0604007].
- [13] J. Gomis and F. Passerini, “Wilson loops as D3-branes,” JHEP **0701**, 097 (2007) [arXiv:hep-th/0612022].
- [14] S. Yamaguchi, “Semi-classical open string corrections and symmetric Wilson loops,” JHEP **0706**, 073 (2007) [arXiv:hep-th/0701052].
- [15] S. A. Hartnoll, “Two universal results for Wilson loops at strong coupling,” Phys. Rev. D **74**, 066006 (2006) [arXiv:hep-th/0606178].
- [16] S. A. Hartnoll and S. P. Kumar, “Higher rank Wilson loops from a matrix model,” JHEP **0608**, 026 (2006) [arXiv:hep-th/0605027].
- [17] N. Drukker, S. Giombi, R. Ricci and D. Trancanelli, “On the D3-brane description of some $1/4$ BPS Wilson loops,” JHEP **0704**, 008 (2007) [arXiv:hep-th/0612168].
- [18] K. Okuyama and G. W. Semenoff, “Wilson loops in $N = 4$ SYM and fermion droplets,” JHEP **0606**, 057 (2006) [arXiv:hep-th/0604209].
- [19] D. E. Berenstein, R. Corrado, W. Fischler and J. M. Maldacena, “The operator product expansion for Wilson loops and surfaces in the large N limit,” Phys. Rev. D **59**, 105023 (1999) [arXiv:hep-th/9809188].

- [20] G. W. Semenoff and K. Zarembo, “More exact predictions of SUSYM for string theory,” Nucl. Phys. B **616**, 34 (2001) [arXiv:hep-th/0106015].
- [21] S. Giombi, R. Ricci and D. Trancanelli, “Operator product expansion of higher rank Wilson loops from D-branes and matrix models,” JHEP **0610**, 045 (2006) [arXiv:hep-th/0608077].
- [22] G. W. Semenoff and D. Young, “Exact 1/4 BPS loop: Chiral primary correlator,” Phys. Lett. B **643**, 195 (2006) [arXiv:hep-th/0609158].
- [23] V. Pestun, “Localization of gauge theory on a four-sphere and supersymmetric Wilson loops,” arXiv:0712.2824 [hep-th].
- [24] N. Drukker, S. Giombi, R. Ricci and D. Trancanelli, “More supersymmetric Wilson loops,” Phys. Rev. D **76**, 107703 (2007) [arXiv:0704.2237 [hep-th]].
- [25] T. T. Wu, “Two-Dimensional Yang-Mills Theory In The Leading 1/N Expansion,” Phys. Lett. B **71**, 142 (1977).
- [26] S. Mandelstam, “Light Cone Superspace And The Ultraviolet Finiteness Of The N=4 Model,” Nucl. Phys. B **213**, 149 (1983).
- [27] G. Leibbrandt, “The Light Cone Gauge In Yang-Mills Theory,” Phys. Rev. D **29**, 1699 (1984).
- [28] N. Drukker, S. Giombi, R. Ricci and D. Trancanelli, “Wilson loops: From four-dimensional SYM to two-dimensional YM,” arXiv:0707.2699 [hep-th].
- [29] N. Drukker, S. Giombi, R. Ricci and D. Trancanelli, “Supersymmetric Wilson loops on S^3 ,” arXiv:0711.3226 [hep-th].
- [30] N. Drukker, “1/4 BPS circular loops, unstable world-sheet instantons and the matrix model,” JHEP **0609**, 004 (2006) [arXiv:hep-th/0605151].
- [31] M. Staudacher and W. Krauth, “Two-dimensional QCD in the Wu-Mandelstam-Leibbrandt prescription,” Phys. Rev. D **57**, 2456 (1998) [arXiv:hep-th/9709101].
- [32] A. Bassetto and L. Griguolo, “Two-dimensional QCD, instanton contributions and the perturbative Wu-Mandelstam-Leibbrandt prescription,” Phys. Lett. B **443**, 325 (1998) [arXiv:hep-th/9806037].
- [33] E. Witten, “On quantum gauge theories in two-dimensions,” Commun. Math. Phys. **141**, 153 (1991).
- [34] E. Witten, “Two-dimensional gauge theories revisited,” J. Geom. Phys. **9**, 303 (1992) [arXiv:hep-th/9204083].
- [35] M. R. Douglas and V. A. Kazakov, “Large N phase transition in continuum QCD in two-dimensions,” Phys. Lett. B **319**, 219 (1993) [arXiv:hep-th/9305047].

- [36] D. J. Gross and A. Matytsin, “Instanton induced large N phase transitions in two-dimensional and four-dimensional QCD,” Nucl. Phys. B **429**, 50 (1994) [arXiv:hep-th/9404004].
- [37] A. Bassetto, L. Griguolo, F. Pucci and D. Seminara, “Supersymmetric Wilson loops at two loops,” arXiv:0804.3973 [hep-th].